eNeuro

Research Article: New Research | Development

Pannexin 1 regulates network ensembles and dendritic spine development in cortical neurons

Juan C. Sanchez-Arias[1], Mei Liu[1], Catherine S.W. Choi[1], Sarah N. Ebert[1], Craig E. Brown[1] and Leigh Anne Swayne[1]

[1]*Division of Medical Sciences, University of Victoria, Victoria, British Columbia V8P 5C2, Canada*

https://doi.org/10.1523/ENEURO.0503-18.2019

Received: 20 December 2018

Revised: 13 May 2019

Accepted: 14 May 2019

Published: 22 May 2019

Author contributions: J.S.-A., M.L., C.C., and L.A.S. designed research; J.S.-A., M.L., C.C., and S.E. performed research; J.S.-A., M.L., C.C., S.E., and L.A.S. analyzed data; J.S.-A., M.L., C.E.B., and L.A.S. wrote the paper.

Funding: Gouvernement du Canada | Canadian Institutes of Health Research (CIHR)
MOP142215
;

Funding: The Scottish Rite Charitable Foundation of Canada
15118
;

Funding: Michael Smith Foundation for Health Research (MSFHR)
5900
;

Funding: Canada Foundation for Innovation (CFI)
29462
;

Funding: Ministry of Technology, Innovation and Citizens' Services | British Columbia Knowledge Development Fund (BCKDF)
804754
.

Conflict of Interest: The authors declare no competing financial interests. A disclosure has been made with the University of Victoria Research Partnerships and Knowledge Mobilization, and a provisional patent application has been filed for a peptide targeting a Panx1-Crmp2 interaction (US Application No. 62/767,806).

This work was supported by operating grants from the Canadian Institutes of Health Research (CIHR Grant MOP142215), The Scottish Rite Charitable Foundation of Canada (15118) and the University of Victoria-Division of Medical Sciences to L.A.S. L.A.S. is also supported by a Michael Smith Foundation for Health Research and British Columbia Schizophrenia Society Foundation Scholar Award (5900). J.C.S.A. was supported by a University of Victoria Fellowship Graduate Award. ML received partial salary support from the Key Laboratory of Neuroregeneration of Jiangsu and Ministry of Education, Co-innovation Center of Neuroregeneration, Nantong University, China. L.A.S. is also grateful for infrastructure support from the Canada Foundation for Innovation (29462) and the BC Knowledge Development Fund (804754) for the Leica SP8 confocal microscope system.

Correspondence should be addressed to Leigh Anne Swayne at lswayne@uvic.ca; twitter: @dr_swayne.

Cite as: eNeuro 2019; 10.1523/ENEURO.0503-18.2019

Pannexin 1 regulates network ensembles and dendritic spine development in cortical neurons

Abbreviated title: Pannexin 1 regulates network ensembles

Juan C. Sanchez-Arias[1], Mei Liu[1,2] Catherine S.W. Choi[1], Sarah N. Ebert[1], Craig E. Brown[1], Leigh Anne Swayne[1*]

[1]Division of Medical Sciences, University of Victoria, Victoria, British Columbia V8P 5C2, Canada,

[2]Key Laboratory of Neuroregeneration of Jiangsu and Ministry of Education, Co-innovation Center of Neuroregeneration, Nantong University, China (*current affiliation*)

Author Contributions

J.C.S.A. and L.A.S. designed research. J.C.S.A., M.L., C.S.W.C., S.N.E. performed research. J.C.S.A., M.L., C.S.W.C., S.N.E., and L.A.S. analyzed research J.C.S.A., M.L., C.E.B., and L.A.S. wrote the manuscript.

Correspondance

*Lead contact. Correspondence: lswayne@uvic.ca; twitter: @dr_swayne

Number of figures: 4 *Note that boxplots were used when the n >3 and was kept consistent within figures (Figure 2 and Figure 4 data are presented with bar graphs with individual points).
Number of tables: 1
Number of words for abstract: 225
Number of words for significance statement: 131
Number of words for introduction: 419
Number of words for discussion: 1,390

Acknowledgements

We are thankful for technical assistance from Maria Weaver, who was supported by a University of Victoria Summer Undergraduate Student Award and Ana De Lucas-Rius.

Declarations

The authors declare no competing financial interests. A disclosure has been made with the University of Victoria Research Partnerships and Knowledge Mobilization, and a provisional patent application has been filed for a peptide targeting a Panx1-Crmp2 interaction (US Application No. 62/767,806).

Funding sources

This work was supported by operating grants from the Canadian Institutes of Health Research (CIHR Grant MOP142215), The Scottish Rite Charitable Foundation of Canada (15118) and the University of Victoria-Division of Medical Sciences to L.A.S. L.A.S. is also supported by a Michael Smith Foundation for Health Research and British Columbia Schizophrenia Society Foundation Scholar Award (5900). J.C.S.A. was supported by a University of Victoria Fellowship Graduate Award. ML received partial salary support from the Key Laboratory of Neuroregeneration of Jiangsu and Ministry of Education, Co-innovation Center of Neuroregeneration, Nantong University, China. L.A.S. is also grateful for infrastructure support from the Canada Foundation for Innovation (29462) and the BC Knowledge Development Fund (804754) for the Leica SP8 confocal microscope system.

ABSTRACT

Dendritic spines are the post-synaptic targets of excitatory synaptic inputs that undergo extensive proliferation and maturation during the first postnatal month in mice. However, our understanding of the molecular mechanisms that regulate spines during this critical period is limited. Previous work has shown that Pannexin 1 (Panx1) regulates neurite growth and synaptic plasticity. We therefore investigated the impact of global Panx1 KO on spontaneous cortical neuron activity using Ca^{2+} imaging and *in silico* network analysis. Panx1 KO increased both the number and size of spontaneous co-active cortical neuron network ensembles. To understand the basis for these findings, we investigated Panx1 expression in postnatal synaptosome preparations from early postnatal mouse cortex. Between 2 and 4 postnatal weeks, we observed a precipitous drop in cortical synaptosome protein levels of Panx1, suggesting it regulates synapse proliferation and/or maturation. At the same time points, we observed significant enrichment of the excitatory postsynaptic density proteins PSD-95, GluA1 and GluN2a in cortical synaptosomes from global Panx1 knockout mice. *Ex vivo* analysis of pyramidal neuron structure in somatosensory cortex revealed a consistent increase in dendritic spine densities in both male and female Panx1 KO mice. Similar findings were observed in an excitatory neuron-specific Panx1 KO line (Emx1-Cre driven; Panx1 cKO^{E}) and in primary Panx1 KO cortical neurons cultured *in vitro.* Altogether, our study suggests that Panx1 negatively regulates cortical dendritic spine development.

KEYWORDS **Pannexin, dendritic spines, cortical neuron, somatosensory, critical period, neurodevelopment, neuronal network ensembles**

SIGNIFICANCE STATEMENT

Our findings reveal an important regulatory role for Pannexin 1 (Panx1) in the formation of connections between nerve cells. We found that removal of the Panx1 altered the ability of nerve cells from the cerebral cortex to fire together. We studied the impact of removing Panx1 on the formation of 'dendritic spines', which are microscopic protrusions that receive information from other nerve cells. We found that removing Panx1 increased the expression of proteins involved in dendritic spine function and also increased the density of dendritic spines on nerve cells of the cerebral cortex. Together these findings suggest Panx1 is a 'brake' on the development of dendritic spines with important implications for the development of nerve cell connections.

INTRODUCTION

Pannexin 1 (Panx1) forms channels permeable to ions and metabolites (as reviewed in Boyce et al., 2018), with modes of activation, channel properties and selectivity currently the subject of intense debate and investigation (Chiu et al., 2018). Nonetheless, Panx1 is enriched in the nervous system, including in neuronal dendrites and spines (Zappala et al., 2006; Zoidl et al., 2007; Weilinger et al., 2012; Cone et al., 2013; Weilinger et al., 2016). Panx1 KO is associated with changes in hippocampal synaptic plasticity (Prochnow et al., 2012; Ardiles et al., 2014).

Several lines of evidence suggest that Panx1 could regulate the formation of neuronal networks or network ensembles, which are groups of spontaneously co-active neurons. Ensembles are emerging as the functional building blocks of cortical activity that underlie sensorimotor integration and learning and memory (for review see Harris et al., 2003; Miller et al., 2014; Carrillo-Reid et al., 2015; Arce-McShane et al., 2016). The formation of synapses plays a major role in the development of network ensembles, providing the structural basis for

higher network connectivity (Jung and Herms, 2014; as reviewed in Hoshiba et al., 2017; Frank et al., 2018). In the rodent cortex, Panx1 transcript levels peak around the time of birth, and then markedly decline during the first four postnatal weeks (Ray et al., 2005; Vogt et al., 2005). This decrease in Panx1 coincides with the critical period for the formation of microscopic protrusions emanating from glutamatergic pyramidal neurons called dendritic spines (Schlaggar et al., 1993; for review see O'Leary et al., 1994; Grutzendler et al., 2002; Trachtenberg et al., 2002; for review see Hensch, 2004; Holtmaat et al., 2005), which receive the majority of excitatory inputs in the brain (as reviewed in Nimchinsky et al., 2002; Alvarez and Sabatini, 2007; Yuste, 2011). Panx1 regulates neurite growth (Wicki-Stordeur and Swayne, 2013) and interacts with collapsin-response mediator protein 2 (Crmp2; Wicki-Stordeur, 2015; Xu et al., 2018), a stable synaptic protein (Heo et al., 2018) that regulates spine development (Zhang et al., 2016).

In order to understand how Panx1 regulates cortical neuron development, we used a multi-level approach involving analyses of network ensembles, synaptic protein expression and dendritic spines in mice with global and glutamatergic-neuron specific Panx1 KO. Panx1 KO cortical cultures showed increased network ensemble formation. Moreover, Panx1 KO cortical synaptosomes exhibited significantly increased expression of excitatory synapse markers (PSD-95, GluA1 and GluN2A) and significantly increased cortical neuron dendritic spine densities. Together our results suggest that Panx1 regulates network ensemble formation by acting as a brake for dendritic spine formation.

MATERIALS AND METHODS

Antibodies

Primary antibodies used in this study were: mouse anti-Gad67 (1:120, MAB5406, Millipore-Sigma), mouse anti-PSD-95 (1:50 for ICC; 1:1500 for WB, MA1-045, Thermo-Fisher), rat anti-GFAP (1:200; 1:2000, 13-0300, Thermo-Fisher), rabbit anti-MAP2 (1:400, ab32454, Abcam), rabbit anti-Panx1 (1:2000 for WB, 91137, Cell Signaling Technologies), rabbit anti-GluA1 (1:2000, 13185, Cell Signaling Technologies), rabbit anti-GluA2 (1:2000, 13604, Cell Signaling Technologies), rabbit anti-GluN1 (1:1000, 5704, Cell Signaling Technologies), rabbit anti-GluN2A (1:1000, ab169873, Abcam), rabbit anti-GluN2B (1:1000, 4207, Cell Signaling Technologies). Secondary antibodies used in this study were: Alexa Fluor® 488-conjugated AffiniPure donkey anti-rabbit IgG (1:600, 711-545-152), Alexa Fluor® 594-conjugated AffiniPure donkey anti-mouse IgG (1:600, 715-585-150), Alexa Fluor® 647-conjugated AffiniPure donkey anti-mouse IgG (1:600, 715-605-150), horseradish peroxidase (HRP)-conjugated AffiniPure donkey anti-rabbit IgG (1:4,000 - 1:8,000; 711-035-152), HRP-conjugated AffiniPure donkey anti-mouse IgG (1:4,000 – 1:8,000; 715-035-150), HRP-conjugated AffiniPure donkey anti-rat (1:4,000 – 1:8,000; 712-035-150). All secondary antibodies were obtained from Jackson ImmunoResearch.

Experimental animals

All animal procedures were performed in accordance with the [Author University] animal care committee's regulations. Male and female mice from postnatal day zero (P0) to P30 (note that P29 and P30 mice were both labelled as P29) were used in this study. Global Panx1 KO and $Panx1^{f/f}$ strains were derived from a strain originally generated by Dr. Valery Shestopalov (Dvoriantchikova et al., 2012) and now also available from the Jackson Laboratory (#026021). Note that the original $Panx1^{f/f}$ 129 strain carried a caspase 4 deletion (Vanden Berghe et al.,

2015). These mice have been back-crossed in-house onto C57BL/6J at least 6 times. Wildtype (WT), Panx1 KO, Panx1$^{f/f}$, and Emx1-Cre;Panx1$^{f/f}$ (cKO^{E}) are on a C57BL/6J background (#000664, the Jackson Laboratory). Panx1 KO mice used for dendritic spine analysis were generated from Panx1$^{+/-}$ breeding pairs (to obtain WT and KO littermates). For conditional KO experiments, breeding pairs consisting of a Panx1$^{f/f}$ male and a Emx1-Cre;Panx1$^{f/f}$ female were used to generate Panx1$^{f/f}$ and Emx1$^{IRES\text{-}Cre}$;Panx1$^{f/f}$ littermates. The Emx1$^{IRES\text{-}cre}$ strain was obtained from the Jackson Laboratory (#005628). Mice were housed under a 12 hours light/dark cycle starting at 8 am, with food and water *ad libitum*; temperature was maintained between 20-25 °C and humidity at 40% - 65%. All animals were weaned at P21 and housed in an enriched environment consisting of crinkle paper, nestlets, one paper hut, and one mouse igloo or mouse tunnel.

Genotyping

Primers for LoxTGF, LoxTGR, and Panx1 LoxR (CTTTGGCATTTTCCCAGTGT, CGCGGTTGTAGACTTTGTCA, and GTCCCTACAGGAGGCACTGA) were used to genotype mice. Identification of mice carrying the Emx1$^{IRES\text{-}Cre}$ transgene was determined using the primers Emx1WTF, Emx1WTR, Generic-CreF, and Generic-CreR (AAGGTGTGGTTCCAG AATCG, CTCTCCACCAGAAGGCTGAG, GCGGTCTGGCAGTAAAAACTATC, GTGAAA CAGCATTGCTGTCACTT). Genomic DNA was extracted from tail clips or ear notches using MyTaq^{TM} Extract-PCR Kit (BIO-21126, Bioline). PCR of DNA from homozygous WT mice amplifies a single 585 bp band, whereas PCR of DNA from homozygous mutant mice have a single 900 bp band, with both bands apparent in PCR samples run using DNA from heterozygous mice; PCR of DNA from Panx1$^{f/f}$ mice have a single 1898 bp band (Dvoriantchikova et al.,

2012). PCR of DNA from mice carrying a single copy of Emx1$^{IRES\text{-}cre}$ transgene have both a 378 bp band (WT) and a 102 bp band (Cre), whereas PCR of DNA from those not carrying the Emx1$^{IRES\text{-}Cre}$ transgene have a single 378 bp band.

Tissue processing and diolistic labelling

Experiments were performed similar to previously described (Brusco et al., 2010; Staffend and Meisel, 2011). Mice were perfused transcardially with 0.1 M PBS followed by 1.5% paraformaldehyde (PFA) in 0.1 M PBS for 30-60 seconds. The dissected brains were immersed in 1.5% paraformaldehyde for 60 minutes and then transferred to 0.1 M PBS. DiI (1,1′-Dioctadecyl-3,3,3′,3′-tetramethylindocarbocyanine perchlorate; 42364 Millipore-Sigma) crystals were placed on the dorsolateral surface of the brains and incubated overnight at 37°C in 1.5% PFA. The tissue was fixed with 4% PFA for 30 minutes at room temperature (RT), followed by 3 washes with 0.1 M PBS and coronally-sectioned on a vibratome (150 µm). Hoechst 33342 (1:500 in 0.1 M PBS, Thermo-Fisher) was used as a nuclear counterstain.

Dendritic spine analysis in brain sections

Note that imaging and analysis were performed blind to the genotype of the groups. High resolution 1498 X 1498 image stacks (75.94 nm/pixel; 0.5 µm z-steps) were captured using a Leica SP8 confocal microscope with 561 nm laser illumination and a 40X/1.30NA oil objective and 2.6X digital zoom. The laser power and gain were manually adjusted to prevent oversaturation of pixel intensity values in the apical dendrite. The analysis was carried out with NIH Image J v.148 (Schneider et al., 2012, https://imagej.nih.gov/ij/) and was restricted to primary apical dendrites on their trajectory through Layers 2/3. Apical shafts were selected for

analysis according to the following criteria: 1) The diolistic label reached the soma of a layer 5 pyramidal cell, and 2) the shaft measured 2-4 µm wide, and 3) at least 100 µm of the shaft was clearly discernible from surrounding cells/shafts. Spines were manually traced through z-sections from the head to their origin on the shaft, considering the following: i) they protruded from the shaft by at least 0.4 µm and ii) they were separated by at least 4 µm from a neighbouring apical dendrite. The spines of 6 apical dendrites that matched these criteria were analyzed for each animal. The spine density was defined as the number of spines per 10 µm and was calculated by dividing the total number of spines by the length of the apical dendrite in µm multiplied by 10. Representative images were processed uniformly with a Gaussian blur of 0.5 pixels, and uniform adjustments to levels and contrast were made using Photoshop CS6 Extended suite (Adobe Systems, Inc.).

Primary cortical neuron cultures

Cortices from P0 WT and Panx1 KO pups of either sex were micro-dissected, chopped with a razor blade and incubated with papain (150 µg/L, P4762, Millipore-Sigma), dispase I (150 µg/L, D4818, Millipore-Sigma), and DNAse 1 (100 µg/L, 10104159001, Roche) for 40 minutes, followed by mechanical dissociation in DMEM/F12 medium supplemented with Neurocult™ SM1 supplement (05711, STEMCELL Technologies), and L-glutamine (200 mM, 07100, STEMCELL Technologies), and penicillin/streptomycin (P/S, 0.1 U/mL, 15140122, Gibco). Cells were plated at a density of 2.5 X 10^5 cells per cm^2 on poly-D-lysine (PDL) pre-coated glass coverslips (GG-12-1.5-PDL, NeuVitro) or Nunc™ LabTek™ Chamber Slide™ systems (154534PK, Thermo-Fisher) for MTT assays. The medium was replaced with Neurocult™ medium (STEMCELL Technologies, 05700) supplemented with SM1 and L-glutamine, P/S, and

gentamicin (0.1 mg/mL, G1397, Millipore-Sigma). From 4 days *in vitro* (DIV) onwards, partial (half) the medium was replenished with new BrainPhys™ maturation medium (Bardy et al., 2015) supplemented with SM1 and Cytosine β-D-arabinofuranoside (ara-C, C1768, Millipore-Sigma) every third day.

Immunostaining and spiny protrusions analysis in cultured neurons

Primary cortical neurons were fixed in 4% EM-grade paraformaldehyde solution pre-warmed to 37°C for 10 min, followed by a washed in PBS and permeabilization with 0.25% Triton X-100 in PBS (PBST) for 10 min at RT, washed again with PBS and then blocked with 10% donkey serum (DS, 017-000-121, Jackson Immunoresearch), 1% BSA, and 22.52 mg/mL glycine in PBST for 30 minutes at RT. Following blocking, cultures were incubated with primary antibodies in 1% BSA, and 5% DS in PBST overnight at 4 °C, washed in PBS three times (10 min), and incubated with secondary antibodies and Alexa Fluor 555 phalloidin (A34055, Invitrogen) in PBST supplemented with 1% BSA, and 5% DS for 1 h at RT. After three washes (10 min), coverslips were mounted on microscope slides using Vectashield Antifade Mounting Medium (H-1000, Vectorlabs). Hoechst 33342 (H3570, Invitrogen) was used as nuclear stain. For the analysis of spiny protrusions and PSD-95+ dendritic spines, high resolution (2048 X 2048, pixel size 0.090 µm) images of neurons were captured using a Leica SP8 confocal microscope (63X/1.20NA). The same acquisition parameters were maintained for all cells across all separate cultures within an experiment. Dendritic spines were defined as actin-enriched protrusions ranging from 0.4 µm and 10 µm in length that emanated directly from the dendritic shaft. Using ImageJ, the longest dendrite of each cell was selected and defined as the primary neurite. Within the primary neurite, a 20 µm segment from the distal tip of the primary neurite

was traced and dendritic spines within the segment were traced with individual ROIs; spine density was defined as the number of spines per 10 µm and was calculated by dividing the total number of spines traced by length of the apical dendrite in µm multiplied by 10. For cell-type characterization of neuronal cultures, coverslips were stained with the protocol described above and primary antibodies (MAP2, Gad67, and GFAP) were incubated overnight at 4 °C, followed by three 10 min washes in PBS, secondary antibody incubation at room temperature, and three more 10 min washes before mounting the coverslips with Vectashield. Images (1024 x 1024, pixel size 0.568 µm, 0.34 mm^2) were captured with a Leica SP8 confocal microscope (20X/0.7NA). The proportion of astrocytes and inhibitory cells were calculated based on GFAP and Gad67 immunoreactivity relative to the total amount of cells. The proportion of excitatory cells was determined from MAP2(+)/Gad67(-) relative to the total amount of cells. Representative images were uniformly adjusted with Gaussian blur (2 pixels), and mild uniform adjustments to levels and contrast using Photoshop CS6 Extended suite (Adobe Systems, Inc.).

Neuronal network analysis in primary cortical neuron cultures

For Ca^{2+} imaging experiments, DIV12-14 neuronal cultures were washed with HBSS and incubated in in BrainPhys™ maturation medium supplemented 4 µM Fluo-4 AM (F14201, Thermo-Fisher,) for 40 minutes at 37°C, 5% CO_2, and 95% humidity. Coverslips were washed, transferred to a 35 mm dish containing BrainPhys™ without phenol red (05791, STEMCELL Technologies), and incubated in the dark for 30 minutes at 37°C, 5% CO_2 and 95% humidity to allow complete de-esterification of the probe. The dish was then mounted onto a heated chamber held at 37°C, 5% CO2 and images were acquired every 5 seconds for 10 minutes (pixel dwell time 36 ns, streamed at 7.41 Hz, exposure/frame capture time 135 ms,; 120 frames) using a laser-

scanning microscope (Leica SP8) using 471 nm laser illumination (constant 5% laser power) and a 20X objective (NA 0.70). Three fields of view (FOVs) were analyzed per coverslip. Regions of interest (ROIs) were drawn around each soma within each FOV. The raw fluorescence intensity values over time within each ROI were extracted using the Leica Application Suite Software (version 3.1.3.16308, Leica Microsystems); the background signal was determined in areas of the culture lacking neurons and was subtracted from all the intensity records; fluorescence intensity values were exported as .csv files. Two to three coverslips across 3 independent cultures were used for this analysis (WT = 8 coverslips across 3 independent cultures; KO = 7 coverslips across 3 independent cultures). Note that cells exhibiting a range in fluorescence intensity values limited to within 10% of maximal fluorescence intensity across the entire recording (i.e. fluorescence intensity of 90% of maximum or greater) were removed from all subsequent analyses, resulting in a total of 27/1044 cells removed across WT coverslips (2.9%) and 66/1155 cells removed across Panx1 KO coverslips (5.7%). This exclusion criteria allowed us to remove cells with abnormally high fluorescence values that could have confound our analysis; however, it might also eliminated cells with very small calcium transients, skewing our results towards more active cells. Then, the extracted .csv files were processed using the Fluorescence Single Neuron and Network Analysis Package, FluoroSNNAP (https://www.seas.upenn.edu/~molneuro/software.html, University of Pennsylvania), an open-source, interactive plugin for MATLAB (MATLAB R2014a, the Mathworks Inc.) for $\Delta F/F_0$ conversion from raw F data, spike probability inference, and network ensemble analysis. Once the raw fluorescence .csv file is imported, the analysis package generates a mock image or stack by randomly placing all the traced ROIs contained in the .csv file, which serves to interact with the imported data by selecting individual ROIs and visualizing their time-varying traces. By

selecting the option "Convert raw fluorescence data to deltaF/F" the difference in fluorescence ($\Delta F/F_0$) was computed by taking the average of all the pixels within each ROI (raw fluorescence trace) and subtracting each value with the mean of the lower 50% values in the previous 10 frames (adjustable parameter), and then dividing that product by the mean of the lower 50% values in the previous 10 frames (Patel et al., 2015). Selection of the module "Infer underlying spike probability" calculates the spike probability of each individual ROI using a fast, non-negative deconvolution method developed by Vogelstein et al. (2010). This inferred spike probability algorithm represents neuronal activity better than $\Delta F/F$ (Vogelstein et al., 2010; Miller et al., 2014). Network ensembles, defined as the group of co-activate neurons in a high-activity frame, were calculated by thresholding spike probability data to 3 standard deviations (SDs) above zero, determined from spike probabilities of the entire population in each FOV; this serves to identify active cells not confounded by noise. Values above the threshold were set to 1, and those below the threshold were set to 0. Then, these binary activity data were shuffled 1,000 times to identify the statistically significant number of groups of co-active neurons, using a significant level of $p<0.05$ (Miller et al., 2014). For distribution analyses the median raw Fluo-4 AM fluorescence intensity (in this case defined as baseline fluorescence) and the difference between maximum and minimum fluorescence intensity values (in this case defined as ΔF, fluorescence intensity range) across all frames were obtained for each ROI (cell) collected in the present study and plotted as relative frequency distributions. Violin plots were generated in RStudio, and distributions were compared using the non-parametric Mann-Whitney *U* test.

MTT cell viability assay

Cell viability was tested in WT and Panx1 KO neuronal cultures Nunc™ LabTek™ Chamber Slide™ using the Vybrant® MTT ([3-(4,5-Dimethylthiazol-2-yl)-2,5-Diphenyltetrazolium Bromide]) cell proliferation Assay Kit (V13154, Thermo-Fisher) and following the manufacturer's instructions. Briefly, 12 mM of MTT stock solution (Component A) were prepared by adding 1 mL of PBS to a 5 mg vial of MTT; 20 µL of this 12 mM MTT solution was added to each well containing neurons bathed in 180 µ L of fresh BrainPhys™ without Phenol Red (05791, STEMCELL Technologies) and incubated for 4 hours at 37 °C and 5% CO_2; wells without neurons were used as negative controls. After this step, ¾ of the medium were removed and 100 µL of DMSO were added in, mixing thoroughly the contents of the well and incubating for 10 minutes at 37 °C. After this, the resulting solution was mixed once again, and the absorbance was read at 540 nm using a microplate reader (Infinite®PRO microplate reader, Tecan Life Sciences). All absorbance values represent the average of 9 scans per well and were normalized to blank wells (wells without neurons). Six wells per culture per group were used for this assay (n = 3 per group).

Synaptosome preparation and Western blotting (WB)

Synaptic proteins were extracted using Syn-PER™ Synaptic Protein Extraction Reagent (87793, Thermo-Fisher) according to the manufacturer's instructions. Briefly, WT and Panx1 KO P14 and P29 cortices were dissected and weighed and then submerged in ice-cold Syn-PER reagent (1mL/100mg) supplemented with protease inhibitor cocktail (P8340, Milipore-Sigma). After homogenization on ice, 10%-20% of the homogenate was stored at -80°C for future analysis; the remaining of the homogenate was centrifuged at 1200 X g for 10 minutes at 4°C. The pellet was discarded, and the supernatant transferred to a new tube, for a new round of centrifugation at

15,000 X g for 20 minutes at 4°C, obtaining synaptosomes. This pellet was resuspended in Syn-PER™ reagent using 150 µL per 100 mg of brain tissue. This synaptosome suspension was stored in 5% (v/v) DMSO at -80°C until analysis. On the day of analysis, 50 µL of the synaptosome suspension was placed in a new tube and centrifuged to collect the pellet. Protein was extracted by adding 200 µL of PBS-based RIPA lysis buffer (1% IGEPAL, 0.5% sodium deoxycholate, 0.1% SDS, supplemented with PI cocktail, PMSF and Na orthovanadate) and immersion in ice for 30 minutes. Samples were heated to 95-100°C for 10 minutes in Laemmli sample buffer, DTT and β−ME before loading 10 µg of protein per lane onto 10% PAGE gels (TGX Stain-Free FastCast Acrylamide Kit 161-0183, Bio-Rad) and protein separation was achieved by application of 200 V. Following electrophoresis, gels were exposed to 30 s UV (G-box imager) to obtain the Stain-free signal (total protein) and then transferred to polyvinyldene fluoride (PVDF) for 1 hour at 100 V. Following this, the Stain-free signal was captured by UV light (5 s), rinsed with deionized water for 30 s, blocked in 5% skim milk in PBS supplemented with 0.1% Tween 20, incubated with primary antibodies at 4°C overnight, and secondary antibodies for 1 h at RT after three washes in PBST. The immunoreactive bands were visualized by enhanced chemiluminescence and quantified using ImageJ (http://imagej.nih.gov/ij/). To determine the cortical specificity and extent of Panx1 KO of the excitatory-specific Panx1 KO model (cKO^{E}), we made whole lysates from the cortices and cerebelli of $Panx1^{f/f}$ and cKO^{E} littermates using PBS-based RIPA lysis buffer and as described above.

Experimental Design and Statistical Analysis

For *ex vivo* analysis (diolistic labeling of dendritic spines) WT and Panx1 KO groups consisted of equal numbers of male and female mice. Note that separate analyses of male and female

groups revealed no sex-specific differences in the overall effects and so the sexes were combined. For *in vitro* experiments, appropriate controls are clearly identified in detail in the figures and figure legends. Treatment timelines and all other relevant details are described in the results and figure legends and where appropriate, illustrated on the figures themselves. Researchers were blinded to the identity of the treatment/experimental groups at all stages of the analysis, except for Western blot analysis. Data are presented as means ± SEM. Significance comparisons were calculated using unpaired Student *t*-test, one-way ANOVA and two-way ANOVA for grouped analyses. Bonferroni's correction was used for multiple comparisons when appropriate. When interactions were statistically significant while using two-way ANOVA for grouped analysis, a simple effect ANOVA with multiple comparison were performed using Bonferroni's correction. For non-normally distributed data we used non-parametric tests. Details of normality tests can be found in Table 1. Statistical significance was determined by a P value <0.05 in all tests used in the present study. Data was analyzed using GraphPad Prism version 6.0d (GraphPad Software, San Diego, CA), and RStudio (version 1.1.463, RStudio Inc). Significance is denoted as $P< 0.05$ (*), $P < 0.01$ (**), $P < 0.001$ (***), $P < 0.0001$ (****). Results of statistical tests are described in detail in the **Table 1**; superscript letters throughout the results section and figure legends indicate the corresponding statistic in the table.

RESULTS

Increased network ensembles and altered Ca^{2+} dynamics in Panx1 KO cortical neurons

To determine the impact of Panx1 on network connectivity, we performed Fluo-4 AM Ca^{2+} imaging in primary cortical neuron cultures from WT and Panx1 KO mice (**Figure 1**). Spontaneous developing networks in cultured cortical neurons exhibit self-sustaining bursts

lasting a few hundred milliseconds occurring at 0.05 Hz to 0.1 Hz between DIV8-21 (Habets et al., 1987; Murphy et al., 1992; Maeda et al., 1995; Tibau et al., 2013). Considering these characteristics and other experimental factors (minimization of phototoxicity, imaging multiple fields-of-view; FOV), we imaged DIV12-14 cultures at 0.2 Hz (pixel dwell time = 36 ns; total frame capture time = 135 ms) for 10 minutes (120 frames). To tease out the effects of Panx1 KO on network properties we performed computational modeling of our Ca^{2+} imaging data using the MATLAB based open-source package, FluoroSNNAP (Fluorescence Single Neuron and Network Analysis Package). FluoroSNNAP allowed us to determine the number and properties of network ensembles, which are defined as a group of neurons that undergo a statistically significant degree of co-activation neurons. These ensembles are identified by their contribution to a so-called 'high-activity frame' characterized by a statistically significant proportion of activated neurons (Miller et al., 2014; Patel et al., 2015). Within this algorithm, statistically significant ($p < 0.05$) high activity frames are identified by comparing the mean activity level of a given frame with a computationally-derived activity threshold calculated using the inferred spike activity data of each cell permutated 1,000 times across the entirety of the recording period).

Figure 1A depicts Fluo-4 and FluoroSNNAP analyses from exemplary FOV and exemplary cells from wildtype (left side) and Panx1 KO (right side) cortical neuron cultures. **Figure 1Ai** depicts two sequential Fluo-4 fluorescence frames captured from an exemplary WT FOV (left side) and an exemplary Panx1 KO FOV (right side) cultured cortical neurons. An increase in Fluo-4 fluorescence intensity in exemplary WT cell #75 highlighted in 'high-activity' frame #27 (on the right) is evident upon comparison with the preceding frame (#26). Similarly, an increase in Fluo-4 fluorescence intensity in exemplary Panx1 KO cell #85 highlighted in 'high-activity' frame #30 (on the right) is evident upon comparison with preceding frame (#29).

The FluoroSNNAP-computed Δ*F/F* (**Figure 1Ai** middle panels) and inferred activity (**Figure 1Ai** bottom panels) of these two exemplary cells is also shown across all frames. **Figure 1Aii** depicts the percent of co-active neurons (top panels) and cell-specific spike activity (raster plot; bottom panels) across all 120 frames from the wildtype (left) and Panx1 KO (right) exemplary FOV. In this exemplary FOV, there are more red crosses (spikes from cells participating in a network ensemble) in the Panx1 KO raster plot. Note that total of 27/1044 cells (2.9%) were removed from WT (2.9%) and 66/1155 cells (5.7%) were from Panx1 KO coverslips according to our exclusion criteria (cells exhibiting sustained fluorescence intensity at 90% of maximum or greater). Consistent with this exemplary data, overall, Panx1 KO cultures exhibited a significant increase in network ensembles (**Figure 1Bi**; $p = 0.0014^{a1}$) and number of cells per ensemble (**Figure 1Bii**; $p < 0.0001^{a2}$), as well as a significant increase in core ensembles (co-active groups of neurons active in more than one network ensemble; **Figure 1Ci**; $p = 0.0071^{b1}$). These changes in network properties were still observed when all the above excluded cells were included. We then looked at raw fluorescence intensity values from Fluo-4 AM labeled primary cortical neurons and plotted the median (defined as baseline for this analysis) and the difference between the maximum and minimum fluorescence intensity values (Δ*F*, fluorescence intensity range) for each neuron recorded during our imaging sessions. Panx1 KO neurons exhibited a significant increase in the baseline intensity of Ca^{2+} transients (**Figure 1D**; $p < 0.0001^{c}$) and range of fluorescence compared to WT neurons (**Figure 1E**; $p < 0.0001^{d}$). Additionally, we examined cell-type composition and cell viability. WT and Panx1 KO DIV12-13 cortical neuron cultures were composed of highly similar percentages of excitatory neurons (~80%), inhibitory neurons (~16%), and astrocytes (2-4%; **Figure 1F**; $p = 0.9702^{e4,8}$, $p = 0.7500^{e5,9}$, $p = 0.1026^{e6,10}$ respectively). The low percentage of interneurons is consistent with previous data from this

developmental timepoint (Habets et al., 1987; Benson et al., 1994; Frega et al., 2014; Johnson et al., 2015). Similarly, cell viability assessed by the conversion of MTT to formazan (MTT assay) was not significantly different between the two groups (**Figure 1G**; $p = 0.9089^{f}$). Taken together, these data suggest that Panx1 KO enhances functional connectivity of developing networks cortical neurons.

Panx1 is enriched in synaptic compartments

To confirm expression of Panx1 in synaptic compartments, P14 cortical synaptosome fractions were prepared and validated by enrichment for PSD-95, and exclusion of the astrocyte protein glial fibrillary acidic protein (GFAP) by Western blotting (**Figure 2A**). The synaptosome fractions demonstrated specific enrichment of Panx1 (**Figure 2Aiii**; $p = 0.0093^{g6,8}$). Western blot analysis of whole cortical lysates from WT (C57BL/6J) mice revealed a dramatic drop in Panx1 expression from P7 to P14, and further, from P14 to P29 (**Figure 2Bii**; $p < 0.0001^{g2}$, $p = 0.0006^{g3}$), consistent with previous reports demonstrating peak Panx1 transcript expression at embryonic day (E) 18 followed by a precipitous postnatal drop (Ray et al., 2005; Vogt et al., 2005).

Increased PSD-95 and altered postsynaptic receptor expression in Panx1 KO cortical synaptosomes

Similar to the changes observed in Panx1 expression in whole cortex lysates, Panx1 expression in cortical synaptosomes dropped significantly (~80%) between P14 and P29 (**Figure 3A, B**; $p < 0.0001^{g3,4,7}$). Panx1 was not detected in cortical synaptosomes from global Panx1 KO mice (**Figure 3A, B**). Consistent with the rapid development of dendritic spines in the first month of

postnatal life (Miller, 1986; Zuo et al., 2005; Romand et al., 2011), expression of PSD-95 increased significantly between P14 and P29 (**Figure 3B**; $p < 0.0001^{h3}$). Somewhat unexpectedly, PSD-95 was further increased in Panx1 KO synaptosomes relative to synaptosomes from age matched WT controls (P14, $p < 0.0001^{h4}$; P29, $p = 0.0220^{h5}$). These changes were accompanied by significant increases in GluA1 and GluN2A in Panx1 KO synaptosomes (**Figure 3B**; $p = 0.0082^{i2}$ and $p = 0.0126^{l2}$, respectively). Interestingly, the developmental increase in GluN1 was more pronounced in WT synaptosomes ($p = 0.0009^{m7}$), while GluN2B levels in Panx1 KO synaptosomes were higher at P14 and showed a more marked developmental decline at P29 ($p = 0.0488^{o3}$, $p = 0.0240^{o5}$). Since the elevated PSD-95 and altered expression of glutamate postsynaptic receptor subunits in Panx1 KO synaptosomes could result from changes in the number of dendritic spines, we next investigated the impact of Panx1 KO on the density of dendritic spines in cortical neurons *ex vivo*.

Increased dendritic spine densities in cortical neurons from Panx1 KO mice

Based on our finding that synaptosomal PSD-95 expression was selectively increased in age-matched Panx1 KO cortical synaptosomes, we tested the hypothesis that Panx1 regulates dendritic spine development. We used the fluorescent lipophilic dye, DiI (1,1′-Dioctadecyl-3,3,3′,3′-tetramethylindocarbocyanine perchlorate), which allows for relatively sparse labelling of somatosensory layer 5 pyramidal neurons (Figure 4A). As predicted, spine densities from the apical dendritic tuft of layer 5 pyramidal neurons were significantly higher in Panx1 global KO mice than age matched WT controls at both P14 and P29 (**Figure 4Bi, Bii**; P14, $p = 0.0014^{p1}$; P29, $p < 0.0001^{q1}$). These changes were consistent with the increased synaptosome PSD-95 expression observed at P14 and P29. Next, because Panx1 has also been detected in astrocytes

(Huang et al., 2007; Iglesias et al., 2009), microglia (Burma et al., 2017), and several vascular system cell types (Begandt et al., 2017) in various contexts, we also generated a conditional glutamatergic neuron-specific (Emx-1$^{IRES-cre}$;Panx1$^{f/f}$) Panx1 KO (Panx1cKO^{E}). Consistent with the global Panx1 KO, spine densities in Panx1cKO^{E} were significantly higher than in Panx1$^{f/f}$ controls (**Figure 4Biii**; p = 0.0104[r1]). The Cre-based recombination in the Emx1-expressing lineage begins as early as E10.5 (Gorski et al., 2002). Western blot analysis (**Figure 4Biv)** of Panx1cKO^{E} and control (Panx1$^{f/f}$) cortical (Cx) and cerebellar (Cb) lysates demonstrates substantial reduction of Panx1 immunoreactivity in Panx1cKO^{E} cortical lysates, confirming Panx1 KO in cortical excitatory neurons (comprise the majority of cortical tissue). Notably, mean spine lengths were not significantly different with either Panx1 KO line, suggesting the additional spines do not represent abnormally long spines or filopodia, (Miller and Peters, 1981; Ziv and Smith, 1996; Zuo et al., 2005; for review see Sala and Segal, 2014). Panx1 KO primary cortical neurons grown in culture for 12 days-in-vitro exhibited significantly higher densities of dendritic protrusions resembling dendritic spines (**Figure 4C**). A similar proportion of dendritic protrusions co-localized with PSD-95 in both wildtype and Panx1 KO cortical neurons and spine lengths were not significantly different between groups. Together these results suggest that deletion of Panx1 in glutamatergic cortical neurons increases spine density in a cell-autonomous way.

DISCUSSION

To our knowledge, this is the first study connecting Panx1 to the structural development of dendritic spines. We observed similar spine lengths and proportions of spines expressing PSD-95 in wildtype and Panx1 KO cortical neurons, suggesting Panx1 KO does not simply induce a

493 selective proliferation of immature spines, but rather increases the number of spines with very
494 similar properties to those found in WT cortical neurons. Our results suggest that this increase in
495 dendritic spine density underlies the larger number of network ensembles observed in Panx1 KO
496 cortical cultures. These findings are consistent with recent evidence demonstrating that
497 incorporation of a cell into a network ensemble requires the development of spines and synapses
498 (Jung and Herms, 2014; as reviewed in Hoshiba et al., 2017; Frank et al., 2018). While cortical
499 cultures, in which we performed our network analysis, are known to contain abundant autaptic
500 connections, these are also highly abundant within the developing rodent neocortex. Lübke et al.
501 (1996) reported that autaptic contacts are found in most layer 5 cortical neurons in situ in the
502 developing rat neocortex (92% of all coupled neurons; 80% of all cells analyzed). Amongst
503 others, a recent report from Yin et al. (2018) confirmed that autapses occur in layer-5 pyramidal
504 neurons in developing mouse prefrontal cortex and human frontal lobe (acute brain slices) that
505 persist into adulthood, promoting neuronal responsiveness, burst firing and coincidence
506 detection. Thus, not only might Panx1 KO impact autapses in culture but also potentially *in vivo*.
507 It is also important to note that our understanding of the contribution of spine development and
508 synaptic strengthening to spontaneous network development is still relatively limited and we
509 cannot yet determine whether the ~20-30% increases in spine density we observed *ex vivo* and *in*
510 *vitro* equates directly to 20-30% increases in the number of synapses. Finally, given that not all
511 synapses/cells are recruited to shape the development of neuronal network ensembles, and since
512 our current understanding of the recruitment process is limited (Hoshiba et al., 2017), in the
513 absence of more sophisticated methodology, we are unable to predict which Panx1 KO cells
514 might be engaged in enhanced coupling. Moreover rescue experiments in which Panx1 is re-

515 expressed in control and Panx1 KO neurons are now needed to determine whether the role of
516 Panx1 in regulating spine formation and network ensembles is direct.

517 The current study expands on previous findings relating to synaptic plasticity in Panx1
518 KO mice by focusing on a different region of the brain, the cortex, and by focus on potential
519 developmental contributions. Previous studies focused primarily on the hippocampal CA1 region
520 at one month of age or older (Prochnow et al., 2012; Ardiles et al., 2014). These studies showed
521 increased CA1 long-term potentiation (LTP) (Prochnow et al., 2009; Ardiles et al., 2014) as well
522 as a reduction in LTD (Ardiles et al., 2014) associated with Panx1 KO; albeit, these effects were
523 observed uniquely in adult animals (3 months for the Prochnow et al. study, 9-12 months for the
524 Ardiles et al. study). Ardiles et al. (2014) found that hippocampal Panx1 expression levels were
525 greatly reduced between young (one month) and older (9-12 month-old) animals, which is
526 consistent with our findings over our earlier age range, and suggest that the decline in Panx1
527 levels begins in the early postnatal period and continues on with increasing age. More recent
528 work showed that Panx1 channels are strongly active under ictal conditions in human brain
529 cortical tissue from epilepsy patients and in the CA1 region of the hippocampus following kainic
530 acid seizure induction (Dossi et al., 2018), suggesting that in pathological conditions Panx1 is
531 positively correlated with excitability; although the mechanistic underpinnings, such as the
532 possible interneuronal or glial contributions to this effect, have not yet been fully resolved.
533 Relatedly, because Panx1 has been detected in multiple cell types and has been associated with
534 cell death processes (reviewed in Sandilos and Bayliss, 2012; Thompson, 2015; Swayne and
535 Boyce, 2017), we analyzed the cellular composition and viability of our cortical cultures.
536 Wildtype and Panx1 KO cultures were comprised of similar percentages of excitatory neurons,
537 inhibitory neurons and astrocytes. The majority of cells in both wildtype and Panx1 KO cultures

were excitatory neurons (~80%). Inhibitory neurons, although less abundant (~16% in our cultures for both wildtype and Panx1 KO), play an important role in shaping cortical networks (Lu et al., 2017). Panx1 has been detected in both excitatory and inhibitory neurons (Ray et al., 2005; Vogt et al., 2005; Zoidl et al., 2007), and this is consistent with our Western blot data from Panx1cKO^{E} (glutamatergic-specific Panx1 KO) and control (Panx1$^{f/f}$) lysates. Cortical control (Panx1$^{f/f}$) lysates exhibited a minor residual Panx1 immunoreactivity which likely reflects expression in inhibitory neurons. While together our results suggest that the impact of Panx1 KO on dendritic spine formation is cell-autonomous (glutamatergic neurons), a potential contribution of inhibitory neuron Panx1 to network ensemble development remains to be determined.

The mechanisms governing spine formation and plasticity are poorly understood (reviewed in Yoshihara et al., 2009; Murakoshi and Yasuda, 2012), and are developmental age and brain region specific, making it difficult to directly compare these previous studies with our own. For example the major chloride extruder in neurons, KCC2, differentially regulates brain-derived neurotrophic factor (BDNF)-dependent dendritic spine development in CA1 and somatosensory neurons during the first postnatal week, (Awad et al., 2018). This study suggests molecular mechanisms of dendritic spine formation in different brain regions might not be completely generalizable. Moreover, mounting evidence implicates Panx1 as a possible chloride permeable channel (Ma et al., 2012; Nomura et al., 2017) and thus this differential regulation and of a chloride extruder could directly impact on Panx1 in spine formation; although it remains to be confirmed whether Panx1 channel function itself is implicated in the regulation of spine development. Further, BDNF, which regulates the brain region-specific effect of KCC2 (Awad et al., 2018), is expressed at higher levels in the hippocampus than in the cortex (Awad et al.,

2018), suggesting fundamental differences in baseline levels of key molecular effectors of synaptic plasticity.

Activity-driven spine stabilization requires PSD-95 (Ehrlich et al., 2007); PSD-95 is more frequently detected at stable rather than transient synaptic contacts (Taft and Turrigiano, 2014), and its overexpression increases synaptic contact stability (El-Husseini et al., 2000). Moreover, most spines lacking a PSD do not persist longer than one day, and further, a reduction in PSD-95 precedes spine loss (Cane et al., 2014). BDNF-dependent PSD-95 delivery into spines requires tubulin polymerization (Hu et al., 2011). Microtubule spine invasion is thought to be necessary for kinesin-based transport of cargo required for spine stabilization (reviewed in Dent, 2017); although the mechanisms regulating this process are still relatively unknown. A recent report described an interaction between Panx1 and Crmp2 (Xu et al., 2018), a protein that regulates microtubule stabilization and elongation (Fukata et al., 2002; Niwa et al., 2017). Block of Panx1 with probenecid reduces the Panx1-Crmp2 interaction and concomitantly results in increased microtubule stability and enhance neurite outgrowth (Xu et al., 2018). Moreover, deletion of Crmp2 reduces dendritic spine density (Zhang et al., 2016). Of note, synaptosome fractions of WT and Panx1 KO cortices at P14 and P29 exhibited similar Crmp2 protein levels (data not shown). Together these findings suggest a working model in which Panx1 sequesters Crmp2 by physical interaction until a specific cue, possibility a local elevation in extracellular ATP (Boyce et al., 2015; Boyce and Swayne, 2017), triggers Panx1 downregulation in the spine/shaft and release of Crmp2 to facilitate microtubule elongation, invasion and delivery of PSD-95 into the spine thereby facilitating associated downstream molecular events associated with spine growth and stability. The role of Panx1-interacting proteins in Panx1 regulation of spine development will be the focus of future studies.

Altogether, our novel findings presented here have implications for understanding neurodevelopment and diseases involving changes in spines. Alterations in dendritic spine densities have been described in a variety of neuropsychiatric disorders (Swann et al., 2000; Kulkarni and Firestein, 2012; Forrest et al., 2018). Of note, a recent study identified a human *PANX1* variant with multi-organ developmental abnormalities associated with marked intellectual disability (Shao et al., 2016). Moreover, single nucleotide polymorphisms affecting Panx1 expression levels have been implicated in ASD (Davis et al., 2012). Therefore, understanding the developmental role of Panx1 could provide important insights into variations in normal brain development as well as risk of neurodegenerative and neuropsychiatric disease.

REFERENCES

Alvarez VA, Sabatini BL (2007) Anatomical and physiological plasticity of dendritic spines. Annu Rev Neurosci 30:79-97.

Arce-McShane FI, Ross CF, Takahashi K, Sessle BJ, Hatsopoulos NG (2016) Primary motor and sensory cortical areas communicate via spatiotemporally coordinated networks at multiple frequencies. Proc Natl Acad Sci U S A 113:5083-5088.

Ardiles AO, Flores-Munoz C, Toro-Ayala G, Cardenas AM, Palacios AG, Munoz P, Fuenzalida M, Saez JC, Martinez AD (2014) Pannexin 1 regulates bidirectional hippocampal synaptic plasticity in adult mice. Front Cell Neurosci 8:326.

Awad PN, Amegandjin CA, Szczurkowska J, Carrico JN, Fernandes do Nascimento AS, Baho E, Chattopadhyaya B, Cancedda L, Carmant L, Di Cristo G (2018) KCC2 Regulates Dendritic Spine Formation in a Brain-Region Specific and BDNF Dependent Manner. Cereb Cortex 28:4049-4062.

Begandt D, Good ME, Keller AS, DeLalio LJ, Rowley C, Isakson BE, Figueroa XF (2017) Pannexin channel and connexin hemichannel expression in vascular function and inflammation. BMC Cell Biol 18:2.

Benson DL, Watkins FH, Steward O, Banker G (1994) Characterization of GABAergic neurons in hippocampal cell cultures. J Neurocytol 23:279-295.

Boyce AK, Kim MS, Wicki-Stordeur LE, Swayne LA (2015) ATP stimulates Pannexin 1 internalisation to endosomal compartments. Biochem J.

Boyce AKJ, Swayne LA (2017) P2X7 receptor cross-talk regulates ATP-induced pannexin 1 internalization. Biochem J 474:2133-2144.

Boyce AKJ, Epp AL, Nagarajan A, Swayne LA (2018) Transcriptional and post-translational regulation of pannexins. Biochim Biophys Acta 1860:72-82.

617 Brusco J, Dall'Oglio A, Rocha LB, Rossi MA, Moreira JE, Rasia-Filho AA (2010) Descriptive
618 findings on the morphology of dendritic spines in the rat medial amygdala. Neurosci Lett
619 483:152-156.
620 Burma NE, Bonin RP, Leduc-Pessah H, Baimel C, Cairncross ZF, Mousseau M, Shankara JV,
621 Stemkowski PL, Baimoukhametova D, Bains JS, Antle MC, Zamponi GW, Cahill CM,
622 Borgland SL, De Koninck Y, Trang T (2017) Blocking microglial pannexin-1 channels
623 alleviates morphine withdrawal in rodents. Nat Med 23:355-360.
624 Cane M, Maco B, Knott G, Holtmaat A (2014) The relationship between PSD-95 clustering and
625 spine stability in vivo. J Neurosci 34:2075-2086.
626 Carrillo-Reid L, Miller JE, Hamm JP, Jackson J, Yuste R (2015) Endogenous sequential cortical
627 activity evoked by visual stimuli. J Neurosci 35:8813-8828.
628 Chiu YH, Schappe MS, Desai BN, Bayliss DA (2018) Revisiting multimodal activation and
629 channel properties of Pannexin 1. J Gen Physiol 150:19-39.
630 Cone AC, Ambrosi C, Scemes E, Martone ME, Sosinsky GE (2013) A comparative antibody
631 analysis of pannexin1 expression in four rat brain regions reveals varying subcellular
632 localizations. Frontiers in pharmacology 4:6.
633 Davis LK, Gamazon ER, Kistner-Griffin E, Badner JA, Liu C, Cook EH, Sutcliffe JS, Cox NJ
634 (2012) Loci nominally associated with autism from genome-wide analysis show
635 enrichment of brain expression quantitative trait loci but not lymphoblastoid cell line
636 expression quantitative trait loci. Mol Autism 3:3.
637 Dent EW (2017) Of microtubules and memory: implications for microtubule dynamics in
638 dendrites and spines. Mol Biol Cell 28:1-8.
639 Dossi E, Blauwblomme T, Moulard J, Chever O, Vasile F, Guinard E, Le Bert M, Couillin I,
640 Pallud J, Capelle L, Huberfeld G, Rouach N (2018) Pannexin-1 channels contribute to
641 seizure generation in human epileptic brain tissue and in a mouse model of epilepsy.
642 Science translational medicine 10.
643 Ehrlich I, Klein M, Rumpel S, Malinow R (2007) PSD-95 is required for activity-driven synapse
644 stabilization. Proc Natl Acad Sci U S A 104:4176-4181.
645 El-Husseini AE, Schnell E, Chetkovich DM, Nicoll RA, Bredt DS (2000) PSD-95 involvement
646 in maturation of excitatory synapses. Science 290:1364-1368.
647 Forrest MP, Parnell E, Penzes P (2018) Dendritic structural plasticity and neuropsychiatric
648 disease. Nat Rev Neurosci 19:215-234.
649 Frank AC, Huang S, Zhou M, Gdalyahu A, Kastellakis G, Silva TK, Lu E, Wen X, Poirazi P,
650 Trachtenberg JT, Silva AJ (2018) Hotspots of dendritic spine turnover facilitate clustered
651 spine addition and learning and memory. Nature Communications 9:422.
652 Frega M, Tedesco M, Massobrio P, Pesce M, Martinoia S (2014) Network dynamics of 3D
653 engineered neuronal cultures: a new experimental model for in-vitro electrophysiology.
654 Scientific reports 4:5489.
655 Fukata Y, Itoh TJ, Kimura T, Menager C, Nishimura T, Shiromizu T, Watanabe H, Inagaki N,
656 Iwamatsu A, Hotani H, Kaibuchi K (2002) CRMP-2 binds to tubulin heterodimers to
657 promote microtubule assembly. Nat Cell Biol 4:583-591.
658 Gorski JA, Talley T, Qiu M, Puelles L, Rubenstein JL, Jones KR (2002) Cortical excitatory
659 neurons and glia, but not GABAergic neurons, are produced in the Emx1-expressing
660 lineage. J Neurosci 22:6309-6314.
661 Grutzendler J, Kasthuri N, Gan WB (2002) Long-term dendritic spine stability in the adult
662 cortex. Nature 420:812-816.

663 Habets AM, Van Dongen AM, Van Huizen F, Corner MA (1987) Spontaneous neuronal firing
664 patterns in fetal rat cortical networks during development in vitro: a quantitative analysis.
665 Exp Brain Res 69:43-52.
666 Harris KD, Csicsvari J, Hirase H, Dragoi G, Buzsaki G (2003) Organization of cell assemblies in
667 the hippocampus. Nature 424:552-556.
668 Hensch TK (2004) Critical period regulation. Annual review of neuroscience 27:549-579.
669 Heo S, Diering GH, Na CH, Nirujogi RS, Bachman JL, Pandey A, Huganir RL (2018)
670 Identification of long-lived synaptic proteins by proteomic analysis of synaptosome
671 protein turnover. Proc Natl Acad Sci U S A 115:E3827-E3836.
672 Holtmaat AJ, Trachtenberg JT, Wilbrecht L, Shepherd GM, Zhang X, Knott GW, Svoboda K
673 (2005) Transient and persistent dendritic spines in the neocortex in vivo. Neuron 45:279-
674 291.
675 Hoshiba Y, Wada T, Hayashi-Takagi A (2017) Synaptic Ensemble Underlying the Selection and
676 Consolidation of Neuronal Circuits during Learning. Front Neural Circuits 11:12.
677 Hu X, Ballo L, Pietila L, Viesselmann C, Ballweg J, Lumbard D, Stevenson M, Merriam E, Dent
678 EW (2011) BDNF-induced increase of PSD-95 in dendritic spines requires dynamic
679 microtubule invasions. J Neurosci 31:15597-15603.
680 Huang Y, Grinspan JB, Abrams CK, Scherer SS (2007) Pannexin1 is expressed by neurons and
681 glia but does not form functional gap junctions. Glia 55:46-56.
682 Iglesias R, Dahl G, Qiu F, Spray DC, Scemes E (2009) Pannexin 1: the molecular substrate of
683 astrocyte "hemichannels". J Neurosci 29:7092-7097.
684 Johnson SE, Hudson JL, Kapur J (2015) Synchronization of action potentials during low-
685 magnesium-induced bursting. J Neurophysiol 113:2461-2470.
686 Jung CK, Herms J (2014) Structural dynamics of dendritic spines are influenced by an
687 environmental enrichment: an in vivo imaging study. Cereb Cortex 24:377-384.
688 Kulkarni VA, Firestein BL (2012) The dendritic tree and brain disorders. Mol Cell Neurosci
689 50:10-20.
690 Lu J, Tucciarone J, Padilla-Coreano N, He M, Gordon JA, Huang ZJ (2017) Selective inhibitory
691 control of pyramidal neuron ensembles and cortical subnetworks by chandelier cells. Nat
692 Neurosci 20:1377-1383.
693 Lubke J, Markram H, Frotscher M, Sakmann B (1996) Frequency and dendritic distribution of
694 autapses established by layer 5 pyramidal neurons in the developing rat neocortex:
695 comparison with synaptic innervation of adjacent neurons of the same class. J Neurosci
696 16:3209-3218.
697 Ma W, Compan V, Zheng W, Martin E, North RA, Verkhratsky A, Surprenant A (2012)
698 Pannexin 1 forms an anion-selective channel. Pflugers Arch.
699 Maeda E, Robinson HP, Kawana A (1995) The mechanisms of generation and propagation of
700 synchronized bursting in developing networks of cortical neurons. J Neurosci 15:6834-
701 6845.
702 McDonald JH (2014) Handbook of Biological Statistics, Third Edition: Sparky House
703 Publishing.
704 Miller JE, Ayzenshtat I, Carrillo-Reid L, Yuste R (2014) Visual stimuli recruit intrinsically
705 generated cortical ensembles. Proc Natl Acad Sci U S A 111:E4053-4061.
706 Miller M, Peters A (1981) Maturation of rat visual cortex. II. A combined Golgi-electron
707 microscope study of pyramidal neurons. J Comp Neurol 203:555-573.

708 Miller MW (1986) Maturation of rat visual cortex. III. Postnatal morphogenesis and
709 synaptogenesis of local circuit neurons. Brain Res 390:271-285.
710 Murakoshi H, Yasuda R (2012) Postsynaptic signaling during plasticity of dendritic spines.
711 Trends Neurosci 35:135-143.
712 Murphy TH, Blatter LA, Wier WG, Baraban JM (1992) Spontaneous synchronous synaptic
713 calcium transients in cultured cortical neurons. J Neurosci 12:4834-4845.
714 Nimchinsky EA, Sabatini BL, Svoboda K (2002) Structure and function of dendritic spines.
715 Annu Rev Physiol 64:313-353.
716 Niwa S, Nakamura F, Tomabechi Y, Aoki M, Shigematsu H, Matsumoto T, Yamagata A, Fukai
717 S, Hirokawa N, Goshima Y, Shirouzu M, Nitta R (2017) Structural basis for CRMP2-
718 induced axonal microtubule formation. Scientific reports 7:10681.
719 Nomura T, Taruno A, Shiraishi M, Nakahari T, Inui T, Sokabe M, Eaton DC, Marunaka Y
720 (2017) Current-direction/amplitude-dependent single channel gating kinetics of mouse
721 pannexin 1 channel: a new concept for gating kinetics. Scientific reports 7:10512.
722 O'Leary DD, Ruff NL, Dyck RH (1994) Development, critical period plasticity, and adult
723 reorganizations of mammalian somatosensory systems. Curr Opin Neurobiol 4:535-544.
724 Patel TP, Man K, Firestein BL, Meaney DF (2015) Automated quantification of neuronal
725 networks and single-cell calcium dynamics using calcium imaging. J Neurosci Methods
726 243:26-38.
727 Prochnow N, Hoffmann S, Vroman R, Klooster J, Bunse S, Kamermans M, Dermietzel R, Zoidl
728 G (2009) Pannexin1 in the outer retina of the zebrafish, Danio rerio. Neuroscience
729 162:1039-1054.
730 Prochnow N, Abdulazim A, Kurtenbach S, Wildforster V, Dvoriantchikova G, Hanske J,
731 Petrasch-Parwez E, Shestopalov VI, Dermietzel R, Manahan-Vaughan D, Zoidl G (2012)
732 Pannexin1 stabilizes synaptic plasticity and is needed for learning. PLoS One 7:e51767.
733 Ray A, Zoidl G, Weickert S, Wahle P, Dermietzel R (2005) Site-specific and developmental
734 expression of pannexin1 in the mouse nervous system. Eur J Neurosci 21:3277-3290.
735 Romand S, Wang Y, Toledo-Rodriguez M, Markram H (2011) Morphological development of
736 thick-tufted layer v pyramidal cells in the rat somatosensory cortex. Front Neuroanat 5:5.
737 Sala C, Segal M (2014) Dendritic spines: the locus of structural and functional plasticity. Physiol
738 Rev 94:141-188.
739 Sandilos JK, Bayliss DA (2012) Physiological mechanisms for the modulation of pannexin 1
740 channel activity. J Physiol 590:6257-6266.
741 Schlaggar BL, Fox K, O'Leary DD (1993) Postsynaptic control of plasticity in developing
742 somatosensory cortex. Nature 364:623-626.
743 Schneider CA, Rasband WS, Eliceiri KW (2012) NIH Image to ImageJ: 25 years of image
744 analysis. Nat Methods 9:671-675.
745 Shao Q, Lindstrom K, Shi R, Kelly J, Schroeder A, Juusola J, Levine KL, Esseltine JL, Penuela
746 S, Jackson MF, Laird DW (2016) A germline variant in PANX1 has reduced channel
747 function and is associated with multisystem dysfunction. J Biol Chem.
748 Staffend NA, Meisel RL (2011) DiOlistic Labeling of Neurons in Tissue Slices: A Qualitative
749 and Quantitative Analysis of Methodological Variations. Front Neuroanat 5:14.
750 Swann JW, Al-Noori S, Jiang M, Lee CL (2000) Spine loss and other dendritic abnormalities in
751 epilepsy. Hippocampus 10:617-625.

752 Swayne LA, Boyce AKJ (2017) Regulation of Pannexin 1 Surface Expression by Extracellular
753 ATP: Potential Implications for Nervous System Function in Health and Disease. Front
754 Cell Neurosci 11:230.
755 Taft CE, Turrigiano GG (2014) PSD-95 promotes the stabilization of young synaptic contacts.
756 Philos Trans R Soc Lond B Biol Sci 369:20130134.
757 Thompson RJ (2015) Pannexin channels and ischaemia. J Physiol 593:3463-3470.
758 Tibau E, Valencia M, Soriano J (2013) Identification of neuronal network properties from the
759 spectral analysis of calcium imaging signals in neuronal cultures. Front Neural Circuits
760 7:199.
761 Trachtenberg JT, Chen BE, Knott GW, Feng G, Sanes JR, Welker E, Svoboda K (2002) Long-
762 term in vivo imaging of experience-dependent synaptic plasticity in adult cortex. Nature
763 420:788-794.
764 Vanden Berghe T, Hulpiau P, Martens L, Vandenbroucke RE, Van Wonterghem E, Perry SW,
765 Bruggeman I, Divert T, Choi SM, Vuylsteke M, Shestopalov VI, Libert C, Vandenabeele
766 P (2015) Passenger Mutations Confound Interpretation of All Genetically Modified
767 Congenic Mice. Immunity 43:200-209.
768 Vogelstein JT, Packer AM, Machado TA, Sippy T, Babadi B, Yuste R, Paninski L (2010) Fast
769 nonnegative deconvolution for spike train inference from population calcium imaging. J
770 Neurophysiol 104:3691-3704.
771 Vogt A, Hormuzdi SG, Monyer H (2005) Pannexin1 and Pannexin2 expression in the developing
772 and mature rat brain. Brain Res Mol Brain Res 141:113-120.
773 Weilinger NL, Tang PL, Thompson RJ (2012) Anoxia-induced NMDA receptor activation opens
774 pannexin channels via Src family kinases. J Neurosci 32:12579-12588.
775 Weilinger NL, Lohman AW, Rakai BD, Ma EM, Bialecki J, Maslieieva V, Rilea T, Bandet MV,
776 Ikuta NT, Scott L, Colicos MA, Teskey GC, Winship IR, Thompson RJ (2016)
777 Metabotropic NMDA receptor signaling couples Src family kinases to pannexin-1 during
778 excitotoxicity. Nat Neurosci 19:432-442.
779 Wicki-Stordeur L (2015) Pannexin 1 regulates ventricular zone neuronal development. In:
780 University of Victoria.
781 Wicki-Stordeur LE, Swayne LA (2013) Panx1 regulates neural stem and progenitor cell
782 behaviours associated with cytoskeletal dynamics and interacts with multiple cytoskeletal
783 elements. Cell Commun Signal 11:62.
784 Xu X, Wicki-Stordeur LE, Sanchez-Arias JC, Liu M, Weaver MS, Choi CSW, Swayne LA
785 (2018) Probenecid Disrupts a Novel Pannexin 1-Collapsin Response Mediator Protein 2
786 Interaction and Increases Microtubule Stability. Front Cell Neurosci 12:124.
787 Yin L, Zheng R, Ke W, He Q, Zhang Y, Li J, Wang B, Mi Z, Long YS, Rasch MJ, Li T, Luan G,
788 Shu Y (2018) Autapses enhance bursting and coincidence detection in neocortical
789 pyramidal cells. Nature communications 9:4890.
790 Yoshihara Y, De Roo M, Muller D (2009) Dendritic spine formation and stabilization. Curr Opin
791 Neurobiol 19:146-153.
792 Yuste R (2011) Dendritic spines and distributed circuits. Neuron 71:772-781.
793 Zappala A, Cicero D, Serapide MF, Paz C, Catania MV, Falchi M, Parenti R, Panto MR, La
794 Delia F, Cicirata F (2006) Expression of pannexin1 in the CNS of adult mouse: cellular
795 localization and effect of 4-aminopyridine-induced seizures. Neuroscience 141:167-178.

796 Zhang H, Kang E, Wang Y, Yang C, Yu H, Wang Q, Chen Z, Zhang C, Christian KM, Song H,
797 Ming GL, Xu Z (2016) Brain-specific Crmp2 deletion leads to neuronal development
798 deficits and behavioural impairments in mice. Nature communications 7.
799 Ziv NE, Smith SJ (1996) Evidence for a role of dendritic filopodia in synaptogenesis and spine
800 formation. Neuron 17:91-102.
801 Zoidl G, Petrasch-Parwez E, Ray A, Meier C, Bunse S, Habbes HW, Dahl G, Dermietzel R
802 (2007) Localization of the pannexin1 protein at postsynaptic sites in the cerebral cortex
803 and hippocampus. Neuroscience 146:9-16.
804 Zuo Y, Lin A, Chang P, Gan WB (2005) Development of long-term dendritic spine stability in
805 diverse regions of cerebral cortex. Neuron 46:181-189.
806

807 **FIGURE LEGENDS**

808

809 **Figure 1**. ***Increased network ensembles and altered Ca^{2+} dynamics in Panx1 KO cortical***
810 ***neurons***

811 ***A.*** Representative analyses for functional connectivity in WT and Panx1 KO primary cortical
812 neuron cultures. Ca2+ imaging data was collected using confocal microscopy in DIV12 primary
813 cortical neurons using Fluo-4-AM. A MATLAB based program called FluoroSNNAP was used
814 to determine network ensemble properties. ***A(i)*** Confocal micrographs of exemplary fields of
815 view (FOVs) of WT and Panx1 KO (labelled as KO) demonstrating Fluo-4-derived Ca^{2+} activity
816 from low and high activity frames (as indicated), along with the FluoroSNNAP output $\Delta F/F$
817 (middle panels) *and* inferred spikes (bottom panels) from the identified WT (#75) and KO (#85)
818 cells. ***A.(ii).*** Percentage of active neurons in each frame from the example FOVs (top panels).
819 The red line indicates the threshold for a statistically significant number of coactive cells in a
820 frame used by FluoroSNNAP (3 standard deviations; SD). Raster plots of WT and KO example
821 FOVs (bottom panels) generated from thresholded spike probability data. Spikes from cells
822 participating in a network ensemble are shown in red. The exemplary high activity frames and
823 cells from part A are also highlighted in red. ***B.*** Network ensemble data from WT and Panx1 KO

DIV12 primary neuron cultures. ***B.(i)***. The mean number of network ensembles was increased in Panx1 KO cultures (WT: 4.0 ± 0.6, KO: 7.6 ± 0.7 network ensembles; $t_{(13)} = 4.1$, $p = 0.0014$[a1]; n = 7-8 coverslips from 3 independent cultures; $^{**}p < 0.01$). ***B(ii).*** The number of cells involved in network ensembles was also increased in Panx1 KO neurons (WT: 5.0 ± 0.6, KO: 8.5 ± 0.6 cell per ensemble; $t_{(13)} = 4.4$, $p < 0.0001$[a2]; n = 20-21 network ensembles from 3 independent cultures; $^{****}p < 0.0001$). ***C.*** Core network ensemble data from WT and Panx1 KO DIV12 primary neuron cultures. ***C(i).*** The mean number of core ensembles (co-activated neurons participating in more than one ensemble) was increased in Panx1 KO cultures (WT: 1.2 ± 0.3, KO: 2.7 ± 0.5 core ensembles; $t_{(39)} = 2.8$, $p = 0.0071$[b1]; n = 20-21 network ensembles from 3 independent cultures; $^{**}p < 0.01$). ***C(ii).*** The number of cells forming a core ensemble was not significant different between the analyzed groups (WT: 3.1 ± 0.3, KO: 3.7 ± 0.3 cells per core ensemble; $t_{(30)} = 1.3$, $p = 0.1968$[b2]; n = 12-20 core ensembles from 3 independent cultures; n.s., not significant). ***D.*** Distributions and violin plots of resting and total change (maximum minus minimum) in Fluo-4 fluorescence intensities in DIV12-14 primary cortical neuronal cultures. ***D(i).*** Frequency distributions of Fluo-4 Ca^{2+} indicator dye fluorescence intensities of WT (red) and Panx1 KO (blue) revealed a right shift towards higher median Ca^{2+} levels at baseline (defined the as raw median fluorescence intensity value for each neuron; WT median = 37, n = 1017 cells; KO median = 58.50, n = 1089 cells; $p < 0.0001$[c]; Mann-Whitney $U = 316{,}969$; data compiled from 7-8 coverslips from 3 independent cultures per condition; $^{****}p < 0.0001$). Dotted lines represent the mean of each distribution; a.u., arbitrary units. ***E.*** Similarly, the difference between the maximum and minimum fluorescence intensity values (ΔF, fluorescence intensity range) was right-shifted and significant larger in Panx1 KO neurons (WT median = 16, n = 1017 cells; KO median = 25, n = 1089 cells; $p < 0.0001$[d]; Mann-Whitney $U = 294{,}294$; data

compiled from a total of 7-8 coverslips across 3 independent cultures per condition; ****$p <$ 0.0001). Dotted lines represent the mean of each distribution; a.u., arbitrary units. ***F.*** WT and Panx1 KO cortical neuronal cultures have a similar cell-type composition. ***F(i).*** Representative images of WT and Panx1 KO cortical neurons labeled with the pan-neuronal marker MAP2, interneuron marker Gad67, and the astrocytic marker GFAP. Scale bar, 100 µm. ***F(ii).*** The proportion of excitatory neurons, inhibitory neurons, and astrocytes was similar between groups (WT excitatory neurons = 81.4% ± 1.3%, KO excitatory neurons = 79.8% ± 1.6%, $p = 0.9702$[e8]; WT inhibitory neurons = 17.1% ± 1.3%, KO inhibitory neurons = 15.2% ± 1.0%, $p = 0.7500$[e9]; WT astrocytes = 1.5% ± 0.4%, KO astrocytes = 4.9% ± 1.0%, $p = 0.1026$[e10], Simple effect ANOVA with Bonferroni's multiple comparison test, n = 16 FOV from 2 independent cultures; n.s., not significant). ***G.***WT and Panx1 cortical neurons have similar cell viability. Conversion of MTT to formazan (absorbance measured at 540 nm) was not significant between groups (WT = 100% ± 2.5%, KO = 98.62% ± 8.5%; $p = 0.9089$[f]; $t_{(4)} = 0.128$; n = 3 independent cultures; n.s., not significant). Data are presented as mean ± SEM.

Figure 2. ***Panx1 is enriched in synaptic compartments***

A. Synaptic protein extraction and isolation reveals Panx1 enrichment in cortical synaptic compartments. ***A(i).*** Protocol for synaptosome preparation from dissected cortical tissue using SynPer™. ***A(ii).*** Western blot of subcellular fractionations obtained from a P14 WT brain and probed with PSD-95 (*top* panel), Panx1 (*second* panel), and GFAP (*third* panel), with Stainfree (total protein) in the bottom panel, demonstrating enrichment of PSD-95 in the P3 fraction (synaptosomes) and exclusion of GFAP (*negative control*). ***A(iii).*** Quantification of Panx1 enrichment in synaptic compartments as determined by higher immunoreactivity in P3

(synaptosomes) relative to homogenate. As expected, PSD-95 was also enriched in P3 (Panx1, $p = 0.0093^{g6,8}$; PSD-95, $p < 0.0001^{g5,7}$; Simple effect ANOVA with Bonferroni's multiple comparison test; n = 3 animals; $^{**}p < 0.01$, $^{****}p < 0.0001$). ***B.*** Panx1 cortical expression is developmentally down regulated ***B(i).*** Western blot of WT dissected whole cortical tissues from P7-P63 animals, probed with Panx1 (*top panel*), and Stainfree (total protein) in the bottom. ***B(ii).*** Panx1 expression decreases with age (age, $F_{(3,8)} = 365.9$, $p < 0.0001^{h1}$; n = 3 animals per group; $^{****}p < 0.0001$) with levels markedly dropping from P7 to P14 ($p < 0.0001^{h2}$; P14-P29, $p = 0.0006^{h3}$; P29-P63, $p = 0.9604^{h4}$; one-way ANOVA with Bonferroni's comparison test; n = 3 animals per age group; $^{***}p < 0.001$; $^{****}p < 0.0001$; n.s., not significant). Data are presented as mean ± SEM.

Figure 3. ***Increased PSD-95 and altered postsynaptic receptor expression in Panx1 KO cortical synaptosomes***

A. Representative Western blots of cortical synaptosome preparations from WT and Panx1 KO (P14 and P29) probed for Panx1, PSD-95, and glutamate postsynaptic receptor subunits (GluA1, GluA2, GluN1, GluN2A, GluN2B). The BioRad Stain-free reagent (bottom panel) was used to quantify total protein for normalization. Molecular weight markers are indicated in kilodaltons (kDa). ***B.*** Expression levels for each protein were normalized to total protein and expressed as a percent of WT P14 values; n = 5 animals per group analyzed in 5 independent experiments. Panx1 significantly decreased from P14 to P29 in WT cortical synaptosomes (P14 = 100 ± 9.4%; P29 = 13.4 ± 1.2%, $p < 0.0001^{i3,4,7}$, simple effect ANOVA with Bonferroni's multiple comparison test; $^{****}p < 0.0001$). No Panx1 signal was detected in Panx1 KO cortical synaptosomes**.** PSD-95 significantly increased with age in both WT and Panx1 KO, and was also

significantly higher in Panx1 KO relative to WT within age-matched controls (age: $F_{(1,16)} = 37.4$, $p < 0.0001$[j3]; genotype: $F_{(1,6} = 175.8$, $p < 0.0001$[j2]; interaction: $F_{(1,16)} = 4.2$, $p = 0.0570$[j1]; two-way ANOVA with Bonferroni's multiple comparison test; WT P14 = 100 ± 8.5%, KO P14 = 179.2 ± 9.1%, $p < 0.0001$[j4]; WT P29 = 248.5 ± 9.0%, KO P29 = 287.9 ± 11.8%, $p = 0.0220$[j5]; *$p < 0.05$, ****$p < 0.0001$).. GluA1 and GluN2a also exhibited age-matched increases in expression in Panx1 KO cortical synaptosomes (GluA1: genotype, $F_{(1,16)} = 9.090$, WT P14 = 100 ± 7.2%, KO P14 = 155.6 ± 24.4%; WT P29 = 93.42 ± 14.9%, KO P29 = 168.4 ± 31.7%, $p = 0.0082$[k2]; GluN2A: $F_{(1,16)} = 7.892$, WT P14 = 100 ± 12.2%, KO P14 = 167.8 ± 31.20%; WT P29 = 121.4 ± 23.2%, KO P29 = 201.3 ± 33.3%,, $p = 0.0126$[n2]), GluN1 developmental upregulation was more pronounced in the WT group ($p = 0.0009$[m1-8]), while GluN2B immunoreactivity was in P14 Panx1 KO synaptosomes with steeper developmental decline at P29 compared to WT (age: $F_{(1,16)} = 4.547$, $p = 0.0488$[o3]; WT P14 = 100 ± 6.5%, WT P29 = 97.1 ± 16.6%, $p > 0.9999$[o4]; KO P14 = 133.1 ± 11.9%, KO P29 = 88.6 ± 5.9%; $p = 0.0014$[o5]; two-way ANOVA with Bonferroni's multiple comparison test; *$p<0.05$). Data are presented as mean ± SEM. For additional statistical information results see **Table 1**[i1-o5].

Figure 4. ***Increased dendritic spine density in Panx1 KO cortical neurons***

A. Experimental set-up for DiI labeling of apical dendrites of layer 5 somatosensory neurons *ex vivo*. On the left is a representative micrograph of a WT P14 mouse cortex labeled on the pial surface with DiI with an overlay delimiting the somatosensory cortex and cortical layers. A yellow arrow denotes the cell bodies of the layer 5 cortical neuron, shown in the inset; scale bar, 100 µm. On the right, a 100 µm segment of the primary apical dendrite of the cell in the inset, traversing layer 2/3; scale bar, 20 µm. Scale bar, 500 µm. ***B.*** Increased dendritic spine density in Panx1 KO cortical neurons. ***B(i).*** Representative maximum intensity projections of Panx1 WT

(left) and Panx1 KO (right) neurons at P14. Scale bar, 1 µm. Average spine density was significantly higher in Panx1 KO (WT, 13.7 ± 0.7 spines per 10 µm; KO, 17.2 ± 0.5 spines per 10 µm, $p = 0.0014^{p1}$; $t_{(14)} = 3.9$, unpaired t-test, n = 8 animals per genotype; $^{**}p < 0.001$). Average spine length was not significantly different (WT, 1.64 ± 0.06 µm; KO, 1.58 ± 0.04 µm, $p = 0.4133^{p2}$; $t_{(14)} = 0.8$, unpaired t-test, n = 8 animals per genotype; n.s., not significant). ***B(ii)***. At P29. average spine density was significantly higher in Panx1 KO (WT, 20.3 ± 0.5 spines per 10 µm; KO, 25.6 ± 0.8 spines per 10 µm; $t_{(12)} = 5.8$, $p < 0.0001^{q1}$, unpaired t-test, n = 7 animals per genotype; $^{****}p < 0.0001$). Average spine length was not significantly different (WT, 1.47 ± 0.01 µm; KO, 1.50 ± 0.03 µm, $p = 0.4274^{q2}$; $t_{(12)} = 0.8$, unpaired t-test, n = 8 animals per genotype; n.s., not significant). ***B(iii).*** Similarly, average spine density was significantly higher at P29 in a conditional excitatory neocortical pyramidal cell Panx1 KO ($Emx1^{IRES\text{-}Cre/+}$;$Panx1^{f/f}$, Panx1 cKO^{E}) when compared to $Panx1^{f/f}$ littermate controls ($Panx1^{f/f}$, 18.2 ± 1.4 spines per 10 µm; cKO^{E}, 25.3 ± 0.8 spines per 10 µm $t_{(4)} = 4.6$; $p = 0.0104^{r1}$, unpaired t-test, n = 3 mice per genotype; $^{*}p < 0.05$). Average spine length was not significantly different ($Panx1^{f/f}$, 1.43 ± 0.03 µm; cKO^{E}, 1.50 ± 0.08 µm, $p = 0.4326^{p2}$; $t_{(4)} = 0.9$, unpaired t-test, n = 3 animals per genotype; n.s., not significant). Data are represented as mean ± SEM. ***C(i).*** Increased dendritic spine density and PSD-95-positive spine density in cultured cortical neurons at DIV12. Representative maximum intensity projections of of primary neurite (longest neurite) distal segments from WT and Panx1 KO cultured cortical neurons. Dendritic spines were identified using the phalloidin (F-actin; blue). PSD-95 puncta (white) were quantified (PSD-95+ spines). Scale bar, 10 µm. ***C(ii).*** Increased mean spine density (WT, 10 ± 0.6 spines per 10 µm; KO, 16 ± 0.5 spines per 10 µm, $t_{(25)} = 8.4$, $p < 0.0001^{s1}$; unpaired t-test, n = 10-17 cells from 3 independent cultures; $^{****}p<0.0001$), and increased of PSD-95+ spines (WT, 1.5 ± 0.3 spines per 10 µm; KO, 3.9 ±

939 0.6 spines per 10 µm, $t_{(25)}$ = 4.2, p = 0.003[s2]; unpaired t-test, n = 10-17 neurons from 3
940 independent cultures; ***p<0.001). Spine length was not different between groups (p =
941 0.2047[s3]). Data are presented as mean ± SEM.
942
943 **Table 1.** ***Statistical table***
944 [‡]Group analyses were performed using two-way ANOVAs. When interactions were significant, a
945 one-way ANOVA with Bonferroni's multiple comparison's test correction was performed to
946 evaluate simple effects (McDonald, 2014).

Figure 1.

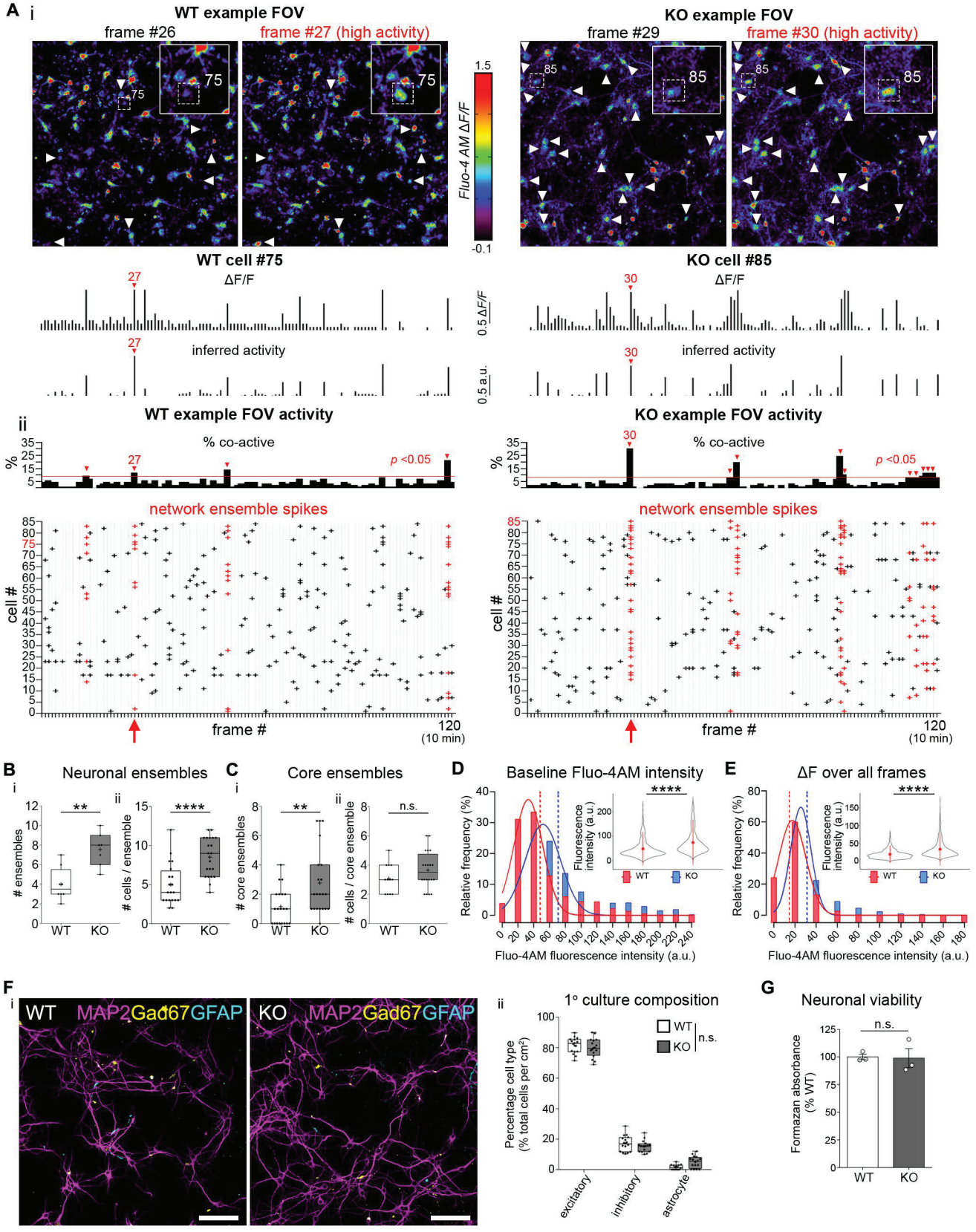

Figure 2.

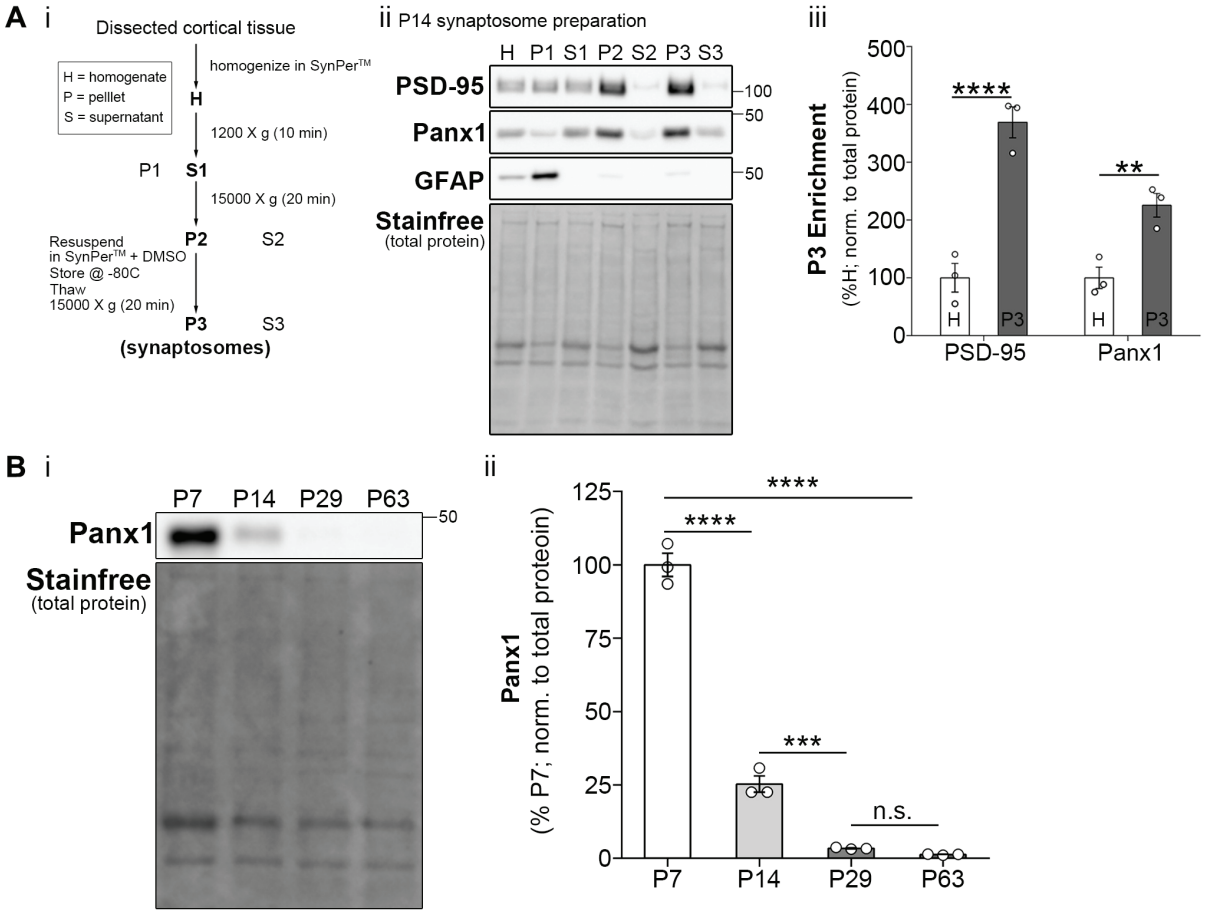

Figure 3.

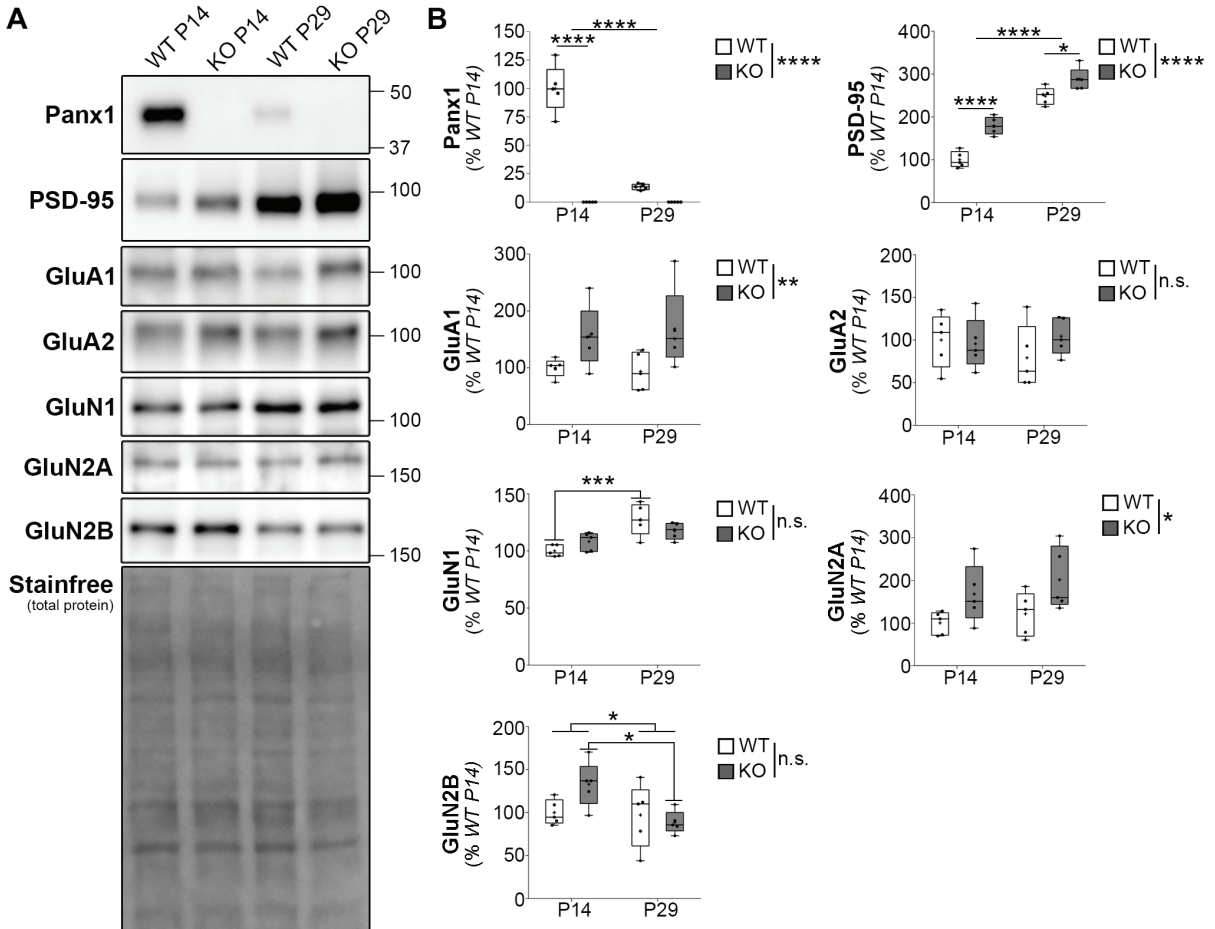

Figure 4.

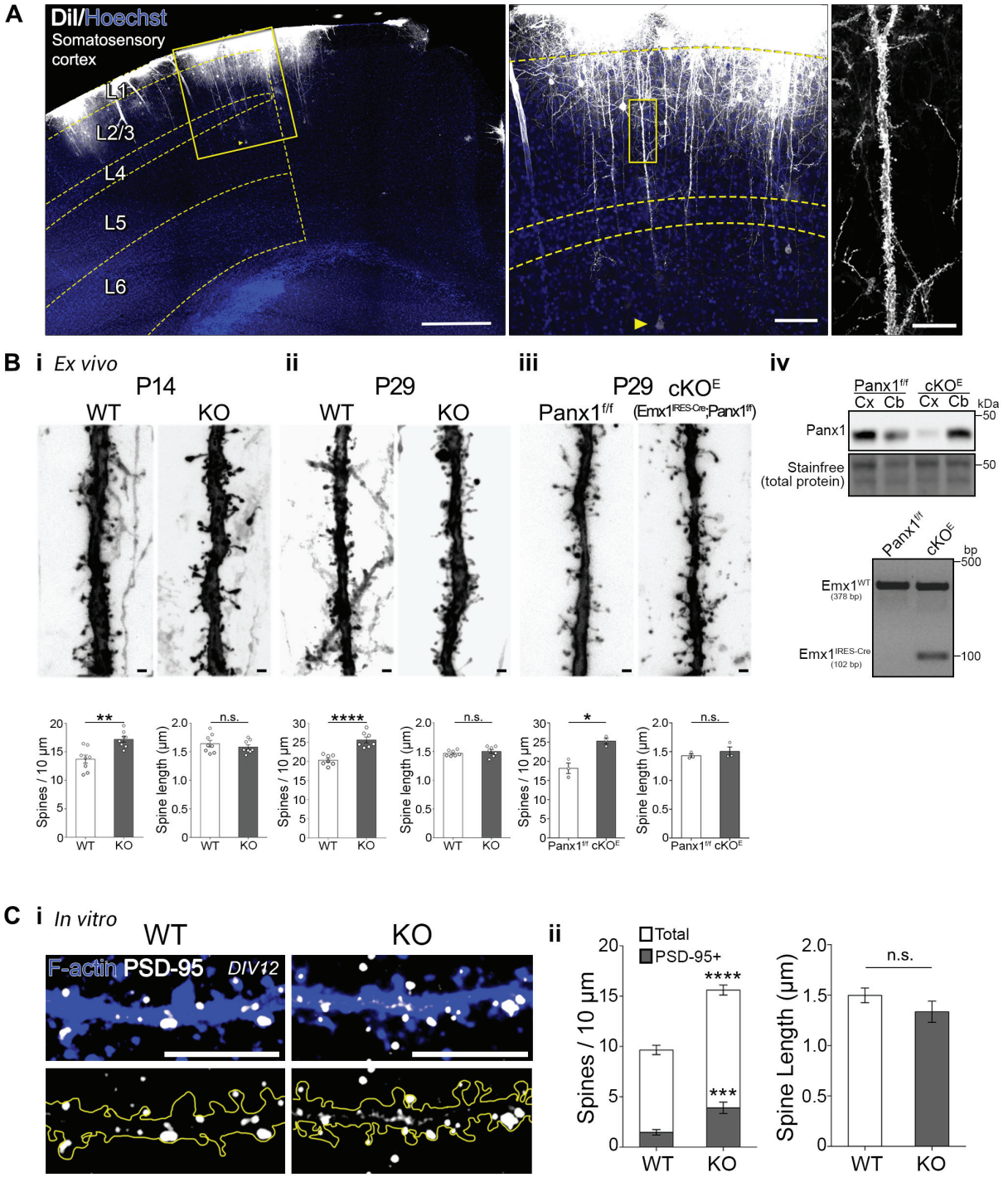

Table 1. Statistical table						
	Figure	Comparison	Data Structure (Shapiro-Wilk normality test unless otherwise stated)	Type of test	Statistic	Confidence, 95% CI
a1	1B(i)	WT vs Panx1 KO	Normal distribution	Unpaired two-tailed *t* test	t = 4.051; df = 13	p = 0.0014; 1.667 to 5.476
a2	1B(i)	WT vs Panx1 KO	Normal distribution (D'Agostino-Pearson Normality Test chosen due to multiple identical values)	Unpaired two-tailed *t* test	i = 4.374; df=39	p < 0.0001; 1.894 to 5.153
b1	1C(i)	WT vs Panx1 KO	Normal distribution (D'Agostino-Pearson Normality Test chosen due to multiple identical values)	Unpaired two-tailed *t* test	t = 2.844; df = 39	p = 0.0071; 0.4654 to 2.758
b2	1C(ii)	WT vs Panx1 KO	Normal distribution	Unpaired two-tailed *t* test	t = 1.320; df = 30	p = 0.1968; -0.3101 to 1.443
c	1D	WT vs Panx1 KO	Not normal (p < 0.0001)	Mann-Whitney *U* test (two-tailed)	U = 316,969	p < 0.0001, 834622, 1.384e6
d	1E	WT vs Panx1 KO	Not normal (p < 0.0001)	Mann-Whitney *U* test (two-tailed)	U = 294,294	p < 0.0001; 811947, 1.407e6
e1	1F(ii)	WT vs Panx1 KO, interaction effect	Normal distribution	Two-way ANOVA	$F_{(2, 90)}$ = 3.475	p = 0.0352
e2	1F(ii)	WT vs Panx1 KO, cell-type effect	Normal distribution	Two-way ANOVA	$F_{(2, 90)}$ = 2615	p < 0.0001
e3	1F(ii)	WT vs Panx1 KO, genotype effect	Normal distribution	Two-way ANOVA	$F_{(1, 90)}$ = 4.934e-008	p = 0.9998
e4	1F(ii)	WT vs Panx1 KO, excitatory neurons	Normal distribution	Two-way ANOVA with Bonferroni's correction		p = 0.9702, -2.347 to 5.568
e5	1F(ii)	WT vs Panx1 KO, inhibitory neurons	Normal distribution	Two-way ANOVA with Bonferroni's correction		p = 0.7500, -2.079 to 5.835
e6	1F(ii)	WT vs Panx1 KO, astrocytes	Normal distribution	Two-way ANOVA with Bonferroni's correction		p = 0.1026, -7.445 to 0.4690
e7	1F(ii)	WT vs Panx1 KO	Normal distribution	Simple effect ANOVA[‡]	$F_{(5, 90)}$ = 1047	p < 0.0001
e8	1F(ii)	WT vs Panx1 KO, excitatory neurons	Normal distribution	Simple effect ANOVA[‡] with Bonferroni's correction		p = 0.9702, -2.347 to 5.568
e9	1F(ii)	WT vs Panx1 KO,	Normal distribution	Simple effect		p = 0.7500,

		inhibitory neurons		ANOVA[‡] with Bonferroni's correction		-2.079 to 5.835
e10	1F(ii)	WT vs Panx1 KO, astrocytes	Normal distribution	Simple effect ANOVA[‡] with Bonferroni's correction		$p = 0.1026$, -7.445 to 0.4690
f	1G	WT vs Panx1 KO Formazan absorbance (MTT conversion to formazan)	Normal distribution	Unpaired two-tailed *t* test	$t = 0.128$ df = 4	$p = 0.9089$, -25.76 to 23.59
g1	2A(iii)	PSD-95 & Panx1 expression in Homogenate (H) vs Synaptosome (P3) content interaction	Normal distribution	Two-way ANOVA	$F_{(1, 8)} = 9.847$	$p = 0.0138$
g2	2A(iii)	PSD-95 & Panx1 expression effect	Normal distribution	Two-way ANOVA	$F_{(1, 8)} = 9.847$	$p = 0.0138$
g3	2A(iii)	H vs P3 content effect	Normal distribution	Two-way ANOVA	$F_{(1, 8)} = 74.46$	$p < 0.0001$
g4	2A(iii)	PSD-95 expression in H vs P3	Normal distribution	Two-way ANOVA with Bonferroni's correction		$p < 0.0001$; -358.0 to -180.1
g5	2A(iii)	Panx1 expression in H vs P3	Normal distribution	Two-way ANOVA with Bonferroni's correction		$p = 0.0093$; -214.5 to -36.58
g6	2A(iii)	PSD-95 & Panx1 expression in H vs P3	Normal distribution	Simple effect ANOVA[‡]	$F_{(3, 8)} = 31.38$	$p < 0.0001$
g7	2A(iii)	Panx1 expression in H vs P3	Normal distribution	Simple effect ANOVA[‡] with Bonferroni's correction		$p < 0.0001$; -214.5 to -36.58
g8	2A(iii)	PSD-95 & Panx1 expression in H & P3	Normal distribution	Simple effect ANOVA[‡] with Bonferroni's correction		$p = 0.0093$; -358.0 to -180.1
h1	2B(iii)	Panx1 expression P7-P63	Normal distribution	One-way ANOVA	$F_{(3, 8)} = 365.9$	$p < 0.0001$
h2	2B(iii)	Panx1 expression P7-14	Normal distribution	One-way ANOVA with Bonferroni's correction		$p < 0.0001$; 0.6377 to 0.8563
h3	2B(iii)	Panx1 expression P14-P29	Normal distribution	One-way ANOVA with Bonferroni's correction		$p = 0.0006$; 0.1161 to 0.3218
h4	2B(iii)	Panx1 expression P29-P63	Normal distribution	One-way ANOVA with Bonferroni's correction		$p = 0.9604$; -0.08815 to 0.1304
i1	3B	Panx1 expression WT vs KO (genotype) by	Normal distribution	Two-way ANOVA	$F_{(1, 16)} = 84.46$	$p < 0.0001$

		age interaction				
i2	3B	Genotype effect	Normal distribution	Two-way ANOVA	$F_{(1, 16)} = 144.7$	$p < 0.0001$
i3	3B	Age effect	Normal distribution	Two-way ANOVA	$F_{(1, 16)} = 84.46$	$p < 0.0001$
i4	3B	Panx1 expression WT P14 vs WT P29	Normal distribution	Two-way ANOVA with Bonferroni's correction		$p < 0.0001$; 70.14 to 103.1
i5	3B	Panx1 expression KO P14 vs KO P29	Normal distribution	Two-way ANOVA with Bonferroni's correction		$p = > 0.9999$; -16.48 to 16.48
i6	3B	Panx1 expression WT P14-29 & KO P14-29	Normal distribution	Simple effect ANOVA[‡]	$F_{(3, 16)} = 104.5$	$p < 0.0001$
i7	3B	Panx1 expression WT P14 vs WT P29	Normal distribution	Simple effect ANOVA[‡] with Bonferroni's correction		$p < 0.0001$, 67.87 to 105.4
i8	3B	Panx1 expression WT P14 % KO 14	Normal distribution	Simple effect ANOVA[‡] with Bonferroni's correction		$p < 0.0001$; 81.25 to 118.7
i9	3B	Panx1 expression WT 29 vs KO P29	Normal distribution	Simple effect ANOVA[‡] with Bonferroni's correction		$p = 0.2476$; -5.369 to 32.13
i10	3B	Panx1 expression KO P14 vs KO P29	Normal distribution	Simple effect ANOVA[‡] with Bonferroni's correction		$p > 0.9999$; -18.75 to 18.75
j1	3B	PSD-95 expression WT vs KO (genotype) by age interaction	Normal distribution	Two-way ANOVA	$F_{(1, 16)} = 4.208$	$p = 0.0570$
j2	3B	Genotype effect	Normal distribution	Two-way ANOVA	$F_{(1, 16)} = 37.42$	$p < 0.0001$
j3	3B	Age effect	Normal distribution	Two-way ANOVA	$F_{(1, 16)} = 175.8$	$p < 0.0001$
j4	3B	PSD-95, WT P14 vs KO P14	Normal distribution	Two-way ANOVA with Bonferroni's correction		$p < 0.0001$; -113.1 to -45.30
j5	3B	PSD-95, WT P29 vs KO P29	Normal distribution	Two-way ANOVA with Bonferroni's correction		$p = 0.0220$; -73.34 to -5.516
k1	3B	GluA1 expression WT vs KO (genotype) by age interaction	Normal distribution	Two-way ANOVA	$F_{(1, 16)} = 0.1996$	$p = 0.6611$
k2	3B	Genotype effect	Normal distribution	Two-way ANOVA	$F_{(1, 16)} = 9.090$	$p = 0.0082$

k3	3B	Age effect	Normal distribution	Two-way ANOVA	$F_{(1, 16)} = 0.02040$	$p = 0.8882$
k4	3B	GluA1, WT P14 vs KO P14	Normal distribution	Two-way ANOVA with Bonferroni's correction		$p = 0.1763$; -131.3 to 20.11
k5	3B	GluA1, WT P29 vs KO P29	Normal distribution	Two-way ANOVA with Bonferroni's correction		$p = 0.0526$; -150.6 to 0.7678
l1	3B	GluA2 expression WT vs KO (genotype) by age interaction	Normal distribution	Two-way ANOVA	$F_{(1, 16)} = 1.156$	$p = 0.2982$
l2	3B	Genotype effect	Normal distribution	Two-way ANOVA	$F_{(1, 16)} = 0.5621$	$p = 0.4643$
l3	3B	Age effect	Normal distribution	Two-way ANOVA	$F_{(1, 16)} = 0.1894$	$p = 0.6693$
m1	3B	GluN1 expression WT vs KO (genotype) by age interaction	Normal distribution	Two-way ANOVA	$F_{(1, 16)} = 4.900$	$p = 0.0417$
m2	3B	Genotype effect	Normal distribution	Two-way ANOVA	$F_{(1, 16)} = 0.05221$	$p = 0.8222$
m3	3B	Age effect	Normal distribution	Two-way ANOVA	$F_{(1, 16)} = 19.95$	$p = 0.0004$
m4	3B	GluN1, WT P14 vs KO P14	Normal distribution	Two-way ANOVA with Bonferroni's correction		$p = 0.3590$; -22.63 to 6.241
m5	3B	GluN1, WT P29 vs KO P29	Normal distribution	Two-way ANOVA with Bonferroni's correction		$p = 0.2069$; -4.355 to 24.52
m6	3B	GluN1 expression WT P14-29 & KO P14-29	Normal distribution	Simple effect ANOVA‡	$F_{(3, 16)} = 8.300$	$p = 0.0015$
m7	3B	GluN1 expression WT P14-29	Normal distribution	Simple effect ANOVA‡ with Bonferroni's correction		$p = 0.0009$; -43.99 to -11.15
m8	3B	GluN1 expression KO P14-29	Normal distribution	Simple effect ANOVA‡ with Bonferroni's correction		$p = 0.5231$; -25.72 to 7.123
m9	3B	GluN1 expression WT vs KO, P14	Normal distribution	Simple effect ANOVA‡ with Bonferroni's correction		$p = 0.7180$, -24.62 to 8.227
m10	3B	GluN1 expression WT vs KO, P29	Normal distribution	Simple effect ANOVA‡ with Bonferroni's correction		$p = 0.4138$, -6.341 to 26.50
n1	3B	GluN2A expression WT vs KO (genotype) by age interaction	Normal distribution	Two-way ANOVA	$F_{(1, 16)} = 0.05302$	$p = 0.8208$

n2	3B	Genotype effect	Normal distribution	Two-way ANOVA	$F_{(1, 16)} = 7.892$	$p = 0.0126$
n3	3B	Age effect	Normal distribution	Two-way ANOVA	$F_{(1, 16)} = 1.092$	$p = 0.3115$
n4	3B	GluN2A, WT P14 vs KO P14	Normal distribution	Two-way ANOVA with Bonferroni's correction		$p = 0.1739$; -159.7 to 24.14
n5	3B	GluN2A, WT P29 vs KO P29	Normal distribution	Two-way ANOVA with Bonferroni's correction		$p = 0.0945$; -171.8 to 12.03
o1	3B	GluN2B expression WT vs KO (genotype) by age interaction	Normal distribution	Two-way ANOVA	$F_{(1, 16)} = 3.507$	$p = 0.0795$
o2	3B	Genotype effect	Normal distribution	Two-way ANOVA	$F_{(1, 16)} = 1.219$	$p = 0.2859$
o3	3B	Age effect	Normal distribution	Two-way ANOVA	$F_{(1, 16)} = 4.547$	$p = 0.0488$
o4	3B	GluN2B, WT P14 vs WT P29	Normal distribution	Two-way ANOVA with Bonferroni's correction		$p > 0.9999$; -35.97 to 41.75
o5	3B	GluN2B, KO P14 vs KO P29	Normal distribution	Two-way ANOVA with Bonferroni's correction		$p = 0.00240$; 5.644 to 83.37
p1	4B(i)	Spine density WT P14 vs KO P14	Normal distribution	Unpaired two-tailed *t* test	$t = 3.962$; df=14	$p = 0.0014$; -5.368 to -1.597
p2	4B(i)	Spine length WT P14 vs KO P14	Normal distribution	Unpaired two-tailed *t* test	$t = 0.8432$; df=14	$p = 0.4133$; -0.09070 to 0.2082
p3	4B(i)	Spine head diameter WT P14 vs KO P14, total distribution	Not normal	Mann-Whitney *U* test (two-tailed)	$U = 1.474e^7$	$p = 0.0131$
p4	4B(i)	Spine head diameter WT P14 vs KO P14, 25% right tail (> percentile 75)	Not normal	Mann-Whitney *U* test (two-tailed)	$U = 931,253$	$p = 0.4022$.
q1	4B(ii)	Spine density WT P29 vs KO P29	Normal distribution	Unpaired two-tailed *t* test	$t = 5.754$; df=12	$p < 0.0001$; 3.279 to 7.275
q2	4B(iii)	Spine length WT P29 vs KO P29	Normal distribution	Unpaired two-tailed *t* test	$t = 0.8214$; df=12	$p = 0.4274$; -0.05194 to 0.1148
r1	4B(iii)	Spine density $Panx1^{f/f}$ vs Panx1 cKO^E	Normal distribution	Unpaired two-tailed *t* test	$t = 4.548$; df=4	$p = 0.0104$; 2.767 to 11.44
r2	4C(ii)	Spine length $Panx1^{f/f}$ vs Panx1 cKO^E	Normal distribution	Unpaired two-tailed *t* test	$t = 0.8717$;	$p = 0.4326$; -0.1602 to

					df=4	0.3069
s1	4C(ii)	Spine density WT vs KO primary cortical neurons	Normal distribution (D'Agostino-Pearson Normality Test chosen due to multiple identical values)	Unpaired two-tailed *t* test	*t* = 8.336; df=25	*p* <0.0001; 4.482 to 7.424
s2	4C(ii)	PSD-95+ spines WT vs KO primary cortical neurons	Normal distribution (D'Agostino-Pearson Normality Test chosen due to multiple identical values)	Unpaired two-tailed *t* test	*t* = 4.243; df=25	*p* = 0.0003; 1.220 to 3.521
s3	4C(ii)	Spine Length WT vs KO primary cortical neurons	Normal distribution	Unpaired two-tailed *t* test	*t* = 1.302; df=25	*p* = 0.2047; -0.4186 to 0.09428